Cell

Resource

Multiplexed Intact-Tissue Transcriptional Analysis at Cellular Resolution

Graphical Abstract

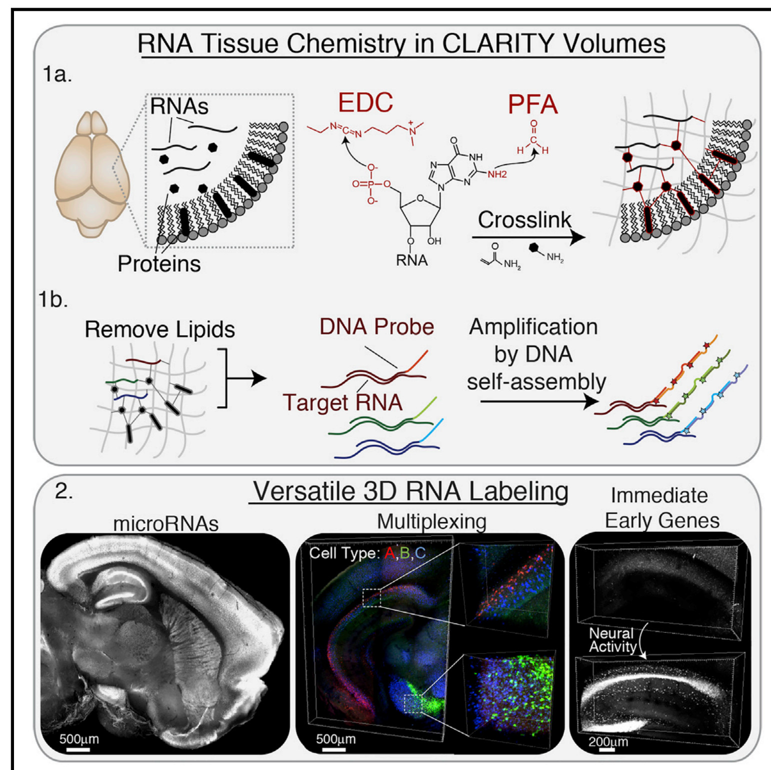

Highlights

- Carbodiimide-based chemistry in CLARITY hydrogels for RNA preservation and detection
- Rapid diffusion of DNA oligonucleotides for volumetric in situ hybridization
- Detection of microRNAs and mRNAs in clarified mouse and human tissues
- DNA-based amplification for multiplexed in situ hybridization in CLARITY

Authors

Emily Lauren Sylwestrak, Priyamvada Rajasethupathy, Matthew Arnot Wright, Anna Jaffe, Karl Deisseroth

Correspondence

deissero@stanford.edu

In Brief

CLARITY with enhanced RNA coupling chemistry is developed for multiplexed, volumetric visualization of both long and short RNAs in a variety of intact tissues.

Sylwestrak et al., 2016, Cell *164*, 792–804
February 11, 2016 ©2016 Elsevier Inc.
http://dx.doi.org/10.1016/j.cell.2016.01.038

CellPress

Cell

Resource

Multiplexed Intact-Tissue Transcriptional Analysis at Cellular Resolution

Emily Lauren Sylwestrak,[1,4] Priyamvada Rajasethupathy,[1,4] Matthew Arnot Wright,[1,2,4] Anna Jaffe,[1]
and Karl Deisseroth[1,2,3,*]
[1]Department of Bioengineering
[2]Department of Psychiatry and Behavioral Sciences
[3]Howard Hughes Medical Institute
Stanford University, 318 Campus Drive, Stanford, CA 94305, USA
[4]Co-first author
*Correspondence: deissero@stanford.edu
http://dx.doi.org/10.1016/j.cell.2016.01.038

SUMMARY

In recently developed approaches for high-resolution imaging within intact tissue, molecular characterization over large volumes has been largely restricted to labeling of proteins. But volumetric nucleic acid labeling may represent a far greater scientific and clinical opportunity, enabling detection of not only diverse coding RNA variants but also non-coding RNAs. Moreover, scaling immunohistochemical detection to large tissue volumes has limitations due to high cost, limited renewability/availability, and restricted multiplexing capability of antibody labels. With the goal of versatile, high-content, and scalable molecular phenotyping of intact tissues, we developed a method using carbodiimide-based chemistry to stably retain RNAs in clarified tissue, coupled with amplification tools for multiplexed detection. The resulting technology enables robust measurement of activity-dependent transcriptional signatures, cell-identity markers, and diverse non-coding RNAs in rodent and human tissue volumes. The growing set of validated probes is deposited in an online resource for nucleating related developments from across the scientific community.

INTRODUCTION

An exciting theme in modern biology is moving toward joint maximization of the content and context of molecular-level observations—that is, obtaining high-resolution and content-rich information about the biological system, while also maintaining this system largely or fully intact to preserve crucial contextual information. Historically, these two goals of content and context have been in opposition, since higher-resolution analyses have tended to require disassembling the system or accepting a limited field of view. But the value of obtaining and integrating information about the identity, function, and connectivity of cells in intact 3D volumes has been increasingly appreciated.

For example, one of the current challenges in neuroscience is to query molecular identity, activity level, and circuit wiring of individual cells within intact brain networks, which would require linkage of information spanning several orders of magnitude in spatial scale. Until recently, investigating the structure of neural networks in this way required sectioning for optical access and molecular labeling, followed by computer-assisted alignment and 3D reconstruction (Denk and Horstmann, 2004; Micheva and Smith, 2007; Oh et al., 2014). Such reconstructions have been valuable, but are often laborious, limited to small volumes, and susceptible to loss of information at section boundaries, making tract-tracing and circuit-mapping particularly difficult (Wanner et al., 2015). However, tissue-clearing techniques have emerged that, to various degrees, enable the visualization of cell morphology (and in some cases, molecular phenotype, as well as local and long-range wiring) embedded within intact neural circuits (Chung et al., 2013; Tomer et al., 2014; Yang et al., 2014; Dodt et al., 2007; Ertürk et al., 2012; Hama et al., 2011; Kuwajima et al., 2013; Renier et al., 2014; Tomer et al., 2015; Richardson and Lichtman, 2015; Staudt et al., 2007; Susaki et al., 2014; Tainaka et al., 2014).

To date, these technologies have chiefly focused on interrogating proteins, whether transgenically expressed or immunohistochemically detected (with the exception of single probes tested in CLARITY-based hydrogel experiments in sectioned tissue; Chung et al., 2013; Yang et al., 2014), and many such approaches may not be compatible with accessing the wealth of biological information contained in the RNA of large intact volumes. This untapped opportunity spans untranslated species, including microRNAs (which, among other reasons for investigation, are particularly relevant to human genetically determined diseases; Esteller, 2011), the majority of splice variants, many immediate early gene (IEG) RNAs used to infer activity of particular regions or cells during behavior (Guzowski et al., 1999; Loebrich and Nedivi, 2009), and even the vast majority of translated gene products, due to limited antibody specificity and availability. We sought to address this challenge by developing generalizable methods for versatile and robust RNA preservation and access within transparent, intact tissue volumes.

RESULTS

Advancing Clarified Tissue Chemistry with Carbodiimide-Based RNA Retention

Many existing clearing methods rely on incubation of tissue for prolonged periods of time at temperatures of 37°C or greater (Chung et al., 2013; Tomer et al., 2014; Yang et al., 2014; Renier et al., 2014; Susaki et al., 2014; Tainaka et al., 2014); however, formalin is known to revert its crosslinks at elevated temperatures, and the bonds made to nucleic acids are particularly vulnerable (Masuda et al., 1999; Srinivasan et al., 2002). Therefore, to improve retention of RNA during high-temperature tissue clearing, we sought to introduce temperature-resistant covalent linkages to RNA molecules prior to clearing by targeting functional groups on the RNA molecule for fixation to surrounding proteins or the hydrogel matrix.

We explored three tissue-chemistry strategies: EDC (1-Ethyl-3-3-dimethyl-aminopropyl carbodiimide) for linkage of the 5′-phosphate group to surrounding amine-containing proteins (Pena et al., 2009; Tymianski et al., 1997); PMPI (p-maleimidophenyl isocyanate) for linkage of the 2′ hydroxyl group to surrounding sulfydryl-containing proteins (Shen et al., 2004); and DSS (disuccinimidyl suberate) for linkage of amine-containing side chains in RNA to surrounding amine-containing proteins (Mattson et al., 1993) (Figure 1A). These crosslinks were introduced after hydrogel embedding (Chung et al., 2013). After fixation, samples were fully cleared and RNA was extracted from each preparation. We observed that, although DSS provided no significant increase in RNA yield (potentially due to overfixation of RNA through multiple amine groups on each RNA molecule), there was markedly improved RNA yield in EDC and PMPI-fixed samples compared with control for both 1% and 4% acrylamide hydrogel compositions (Figure 1B). However, since PMPI doubled tissue-clearing time, while EDC only marginally increased clearing time (1 to 2 extra days in 1 mm tissue blocks), we proceeded with EDC as an RNA-fixation agent for CLARITY.

To complement these quantitative total-RNA biochemical measures with direct visualization of retained RNA within tissue, we stained tissue samples of different hydrogel compositions with acridine orange, an intercalating RNA dye. We found significantly increased RNA staining in EDC fixed samples, with EDC-treated 1% CLARITY tissue showing the best RNA labeling (Figures 1C and 1D). While promising, these total RNA measures did not specifically address mRNA, the population most relevant to molecular phenotyping and activity-dependent gene expression (in contrast to the more abundant rRNA, which, by virtue of tight association with proteins, could contribute disproportionately to the improvement seen with EDC). To determine if EDC improved mRNA preservation, we performed in situ hybridization with a 50 base deoxy-thymine oligonucleotide (oligo(dT)) to target the polyA tail of mature mRNA. Again, we found that 1% CLARITY with EDC samples exhibited the highest RNA signal (Figures 1E and 1F). Surprisingly, the 4% acrylamide hydrogel composition both with and without EDC exhibited significantly reduced RNA detection with both acridine orange staining and oligo(dT) in situ hybridization relative to 1% acrylamide conditions (as well as weaker staining in target-specific in situ hybridization; Figure S1A). This consistent picture may reveal that the dense hydrogel network in 4% CLARITY makes mRNA targets less accessible for probe hybridization. In support of this notion, we find high concentrations (10 M) of EDC also reduced mRNA staining, whereas more modest fixation (0.1 M–1.0 M EDC) provided the most effective labeling of RNAs (Figures 1G and 1H).

A major motivation for RNA detection includes broad application to clinical tissue, but human samples are particularly prone to RNA degradation since pre-fixation post-mortem intervals vary, immersion-fixation crosslinks tissue more slowly than transcardial perfusion, and clinical samples are often banked for extended periods of time. We have also found that human tissue clears more slowly and, in some cases, demands higher clearing temperatures. To test if EDC could improve RNA retention in human tissue, we compared two human samples collected during temporal lobe resection, one treated with EDC and one as an untreated control (1% CLARITY hydrogel). Although both samples showed comparably strong mRNA signal prior to clearing, we found that only the EDC-treated sample exhibited detectable mRNA after clearing (Figures 1I and 1J). We reasoned that EDC might not only be critical for the immediate processing of CLARITY samples, but might also enable long-term storage with little RNA loss. To test this idea, we extracted and measured total RNA from rodent tissue during each stage of the clearing process. After a small loss of RNA during clearing, there was no significant loss during subsequent storage at 4°C for up to 6 months (Figure 1K), demonstrating a surprising level of stability (also reflected in target-specific in situ hybridization; Figure S1B). Together, these data identify and validate a nucleic acid-tuned CLARITY chemistry with EDC.

Quantifying Diffusion of in Situ Hybridization Components into Clarified Tissue

After ensuring stable retention of RNAs, we next focused on access to target RNAs for specific labeling in transparent tissue volumes. Traditional in situ hybridization (ISH) uses labeled DNA or RNA probes, which are detected by enzyme-conjugated antibodies that catalyze the deposition of chromophores or fluorophores at the target location. Interrogation of RNA by these methods requires the penetration of each component to the target location. Since prior work had only shown detection of RNA in small volumes (100–500 μm thick; Chung et al., 2013; Yang et al., 2014), we sought to test the ability of ISH components to diffuse into intact EDC-CLARITY tissue.

We began by characterizing the diffusion of nucleic acid probes into EDC-CLARITY tissue. We incubated tissue blocks with 50-base DIG-labeled DNA or RNA probes and visualized the diffusion profile of these probes by cutting cross-sections through the center of the tissue blocks and quantifying probe density on the newly exposed surface via antibody-based enzymatic amplification (tyramide signal amplification; TSA) (Figure 2A). We found that DNA probes diffused significantly faster into EDC-CLARITY tissue than corresponding RNA probes (Figures 2B–2D); this important effect may be due to greater nonspecific tissue binding of RNA at this temperature, hindering penetration. Strikingly (and with substantial implications for nucleic acid labeling as the potential approach of choice for transparent tissue molecular phenotyping), we consistently observed DNA

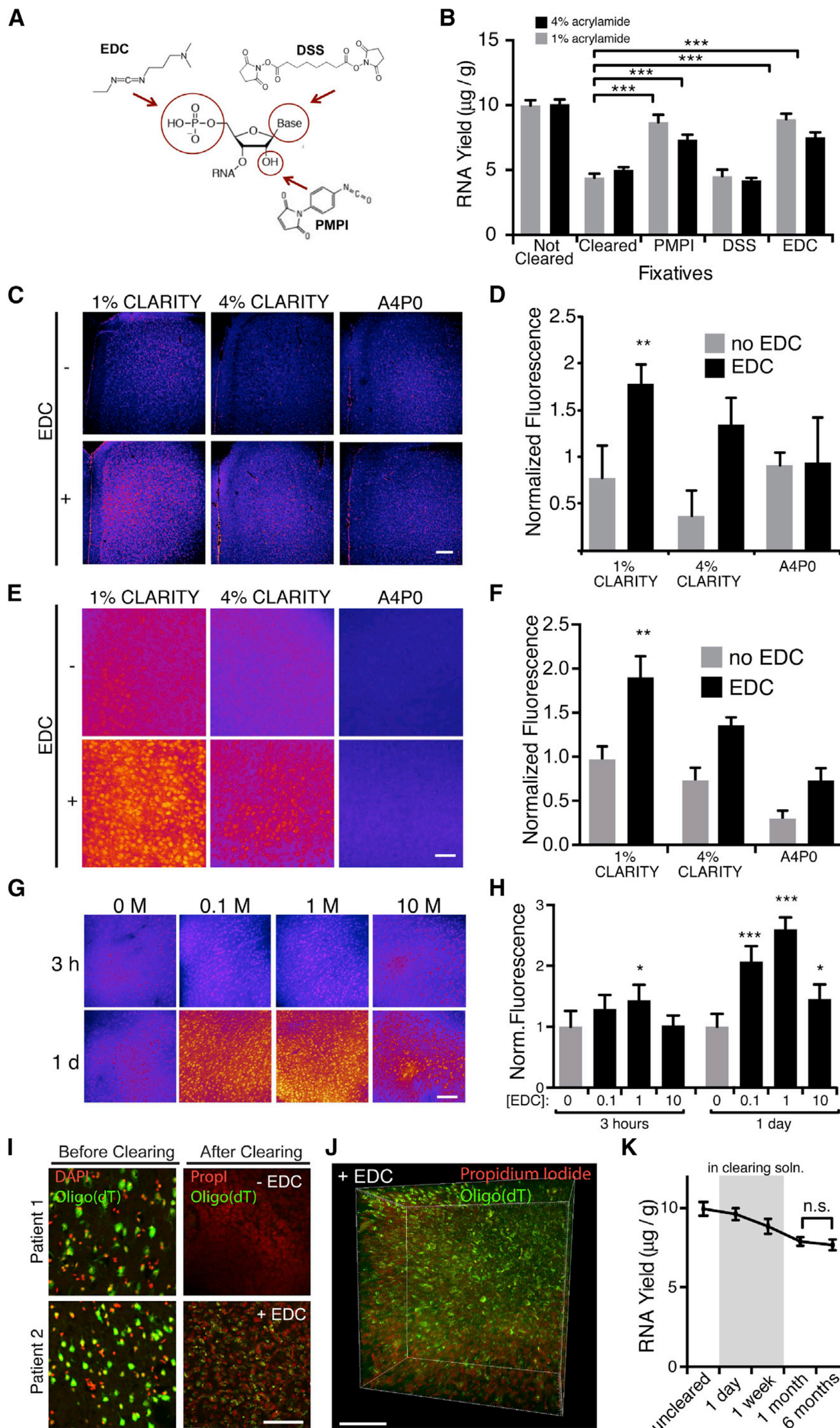

Figure 1. Fixation in EDC Significantly Improves RNA Retention in CLARITY Volumes

(A) Chemical compounds targeting functional groups on RNA (red circles) were characterized and assessed for RNA fixation and retention.

(B) 1 mm mouse brain blocks were embedded in CLARITY hydrogel containing either 1% or 4% acrylamide; then either immediately processed for RNA extraction (labeled "Not Cleared"), or instead post-fixed overnight in PMPI, DSS, EDC, or no-fix (the latter is labeled only as "Cleared" since the last four categories were subsequently put through the CLARITY process until visually transparent and processed for RNA extraction). There was a significant increase in RNA yield in PMPI and EDC-treated groups relative to cleared no-fix controls (***$p < 0.001$, one-way ANOVA, with Sidak's post hoc multiple comparisons test; n = 6 tissue blocks per group).

(C) 1 mm blocks embedded in hydrogel (containing 1% or 4% acrylamide, or 4% acrylamide with no PFA) were post-fixed with EDC (+) or no fix (−) and then cleared and stained with acridine orange to visualize total RNA levels (false colored; RNA signal in pink). Scale bar, 200 µm. Relative intensities are quantified in (D).

(D) 1% hydrogel embedded slices post-fixed in EDC showed significantly more RNA than all other conditions tested. Fluorescence intensities are normalized to mean intensity for all conditions for each experiment (**$p < 0.01$, one-way ANOVA, with Sidak's post hoc multiple comparisons test; n = 5 tissue blocks per group).

(E) 1 mm blocks prepared as in (C), hybridized with an oligo(dT) probe to detect mRNA (false colored). Scale bar, 50 µm. Relative intensities are quantified in (F).

(F) 1% hydrogel embedded slices post-fixed in EDC showed more mRNA than all other conditions tested. Fluorescence intensities are normalized to mean intensity for all conditions for each experiment (**$p < 0.01$, one way ANOVA, Tukey's post hoc test for multiple comparisons; n = 4 tissue blocks per condition).

(G) 1 mm blocks of tissues were embedded in a 1% CLARITY hydrogel and post fixed with 0, 0.1, 1, or 10 M EDC, either for 3 hr or 1 day at 37°C. Oligo(dT) was performed as in (E). Relative intensities are quantified in (H).

(H) Fixation with 0.1 M or 1 M EDC for 1 day produced optimal RNA hybridization in 1% CLARITY tissue. Fluorescence intensities from oligo(dT) are normalized to mean intensity of the no EDC condition. Asterisks indicate statistical significance compared to 0 M EDC, 3 hr condition (***$p < 0.001$, *$p < 0.05$, one way ANOVA, Tukey's post hoc test for multiple comparisons). n = 4 tissue blocks per condition.

(I) In situ hybridization in human tissue from temporal lobe resection. Left, small samples of resection from each patient were PFA fixed and oligo(dT) hybridization was performed to confirm that mRNA was intact before clearing. The remaining tissue was immersion fixed in 1% CLARITY hydrogel (2 days), embedded, then cleared immediately (−EDC), or fixed in EDC overnight at 37°C prior to clearing (+EDC). Right, mRNA was detected by oligo(dT) and DNA was stained with propidium iodide (PropI). Scale bar, 100 µm.

(J) 3D rendering of EDC fixed human temporal lobe volume (same patient as in [G]). Scale bar, 100 µm.

(K) 1 mm tissue blocks (1% hydrogel, EDC postfix) were processed for RNA extraction at various time points: uncleared (immediately after post-fixation); 1 day and 1 week (while in clearing solution); 1 month and 6 months (after clearing and stored in PBST). There is no significant loss of RNA during storage even up to 6 months at 4°C (n = 6 slices per group, n.s. paired t test). All data are means ± SD.

See also Figure S1.

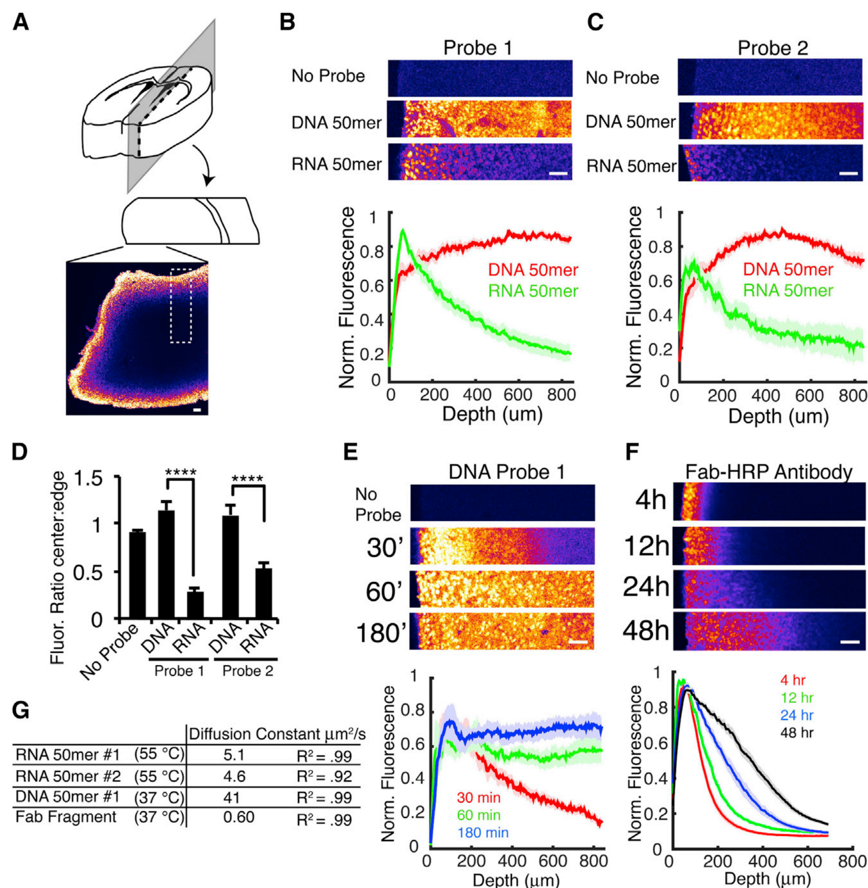

		Diffusion Constant μm²/s	
RNA 50mer #1	(55 °C)	5.1	R^2 = .99
RNA 50mer #2	(55 °C)	4.6	R^2 = .92
DNA 50mer #1	(37 °C)	41	R^2 = .99
Fab Fragment	(37 °C)	0.60	R^2 = .99

Figure 2. DNA Diffuses into CLARITY Tissue More Quickly than Antibodies

(A) Tissue configuration for (B), (C), (E), and (F). 2 mm EDC-CLARITY blocks are incubated in nucleic acid probes or antibody for time indicated and fixed in 4% PFA. 200 μm cross-sections are cut, probe diffusion is detected by TSA on the newly exposed tissue surface, and ROIs are selected as indicated by the dotted box and quantified in (B), (C), (E), and (F).

(B and C) 3 hr incubation with DIG-labeled riboprobes or DNA oligonucleotides (50 bases) targeting two different mRNAs in 50% formamide, 5× SSC at 55°C. Top: example ROIs of tissue as shown in (A), pseudocolored. Cross-section is incubated in anti-DIG Fab fragment antibody conjugated to HRP and detected with TSA using FITC. Bottom: quantification of signal intensity as a function of depth for 10–15 ROIs from 3 experiments. For each ROI, no probe control is subtracted, and signal is normalized to peak intensity.

(D) Quantification of ratio of signal intensity at tissue edge to center, calculated as maximum intensity over first 100 μm to average intensity of last 100 μm. (****$p < 0.0001$, one way ANOVA, Tukey's post hoc test for multiple comparisons).

(E) Diffusion of 50 base DNA oligonucleotide at shorter incubation times with hybridization conditions optimized for in situ hybridization with DNA probes (30, 60, and 180 min; 2× SSC, 40% formamide, 37°C). n = 6–12 ROIs.

(F) Antibody diffusion. CLARITY tissue is incubated in 50 base oligonucleotide probes overnight, washed, and transferred to anti-DIG antibody conjugated to HRP for time indicated. Tissue is sectioned as in (A), and antibody diffusion is detected by TSA. For 4 hr, n = 25 ROIs; 12 hr, n = 8; 24 hr, n = 17; 48 hr, n = 24.

(G) Diffusion constants and R^2 values for nucleic acid and antibody diffusion in CLARITY tissue. Constants calculated by fitting average curves to Fick's Law: $y = n0*\mathrm{erfc}(x/(2*\sqrt{(D*t)}))$ for one dimensional diffusion in a uniform medium with constant boundary condition. Diffusion rate is slower than reported previously in CLARITY tissue (Li et al., 2015), which may arise from additional crosslinking during EDC fixation, or changes in tissue properties during in situ hybridization. Curves used for fitting: RNA, 3 hr incubation; DNA, 30 min incubation; antibody, 4 hr incubation. All error bars indicate SEM. All scale bars, 100 μm.

probes reaching the center of 2 mm tissue blocks within 3 hr. It should be noted that this detection method (TSA) may saturate at higher concentrations and obscure more subtle underlying concentration gradients expected to be present at 1–3 hr time points, but these diffusion rates are still considerably faster than observed for antibodies (Chung et al., 2013; Tomer et al., 2014).

At 37°C (optimized for DNA-RNA hybridization), DNA probes reached the center of a 2-mm-thick block in <1 hr (Figure 2E). In contrast, enzyme-linked Fab antibody fragments penetrated only ~500 μm into tissue even after 2 days (Figure 2F). Importantly, the rate of diffusion for the Fab fragment was almost two orders of magnitude slower than that of the DNA oligonucleotide (Figure 2G) under the EDC-CLARITY-ISH condition. Taken together, these experiments reveal that short DNA probes rapidly diffuse throughout large volumes of EDC-CLARITY tissue and suggest that an optimal approach to labeling native RNA species in large intact volumes could leverage the speed and specificity of short DNA probes in addition to EDC tissue chemistry.

In Situ Hybridization in EDC-CLARITY

Based on these findings that demonstrate stable retention of RNA with EDC-CLARITY and rapid penetration with short DNA probes, we next sought to develop a panel of oligonucleotide-based ISH techniques for application to large transparent tissue volumes. We began with digoxigenin (DIG)-labeled DNA oligonucleotide probes targeting *somatostatin* mRNA (three probes) and amplified with anti-DIG HRP-conjugated antibody and TSA (Figure 3A). In initial tests, we were readily able to resolve individual cells expressing *somatostatin* mRNA, demonstrating that specific mRNA species within the EDC-CLARITY hydrogel can be retained and are accessible to ISH probes (Figure 3C).

However, using this technique in larger volumes revealed two major limitations: (1) the surface of the tissue sections showed non-specific staining that could result in false positives during cell detection, and (2) the signal was visible only to a depth of <300 μm (Figure 3C). A similar pattern was seen in parallel experiments with a probe set targeting *YFP* mRNA in a Thy1-YFP transgenic mouse, confirming that, under these conditions, TSA signal at the tissue surface lacks specificity (Figure S2C).

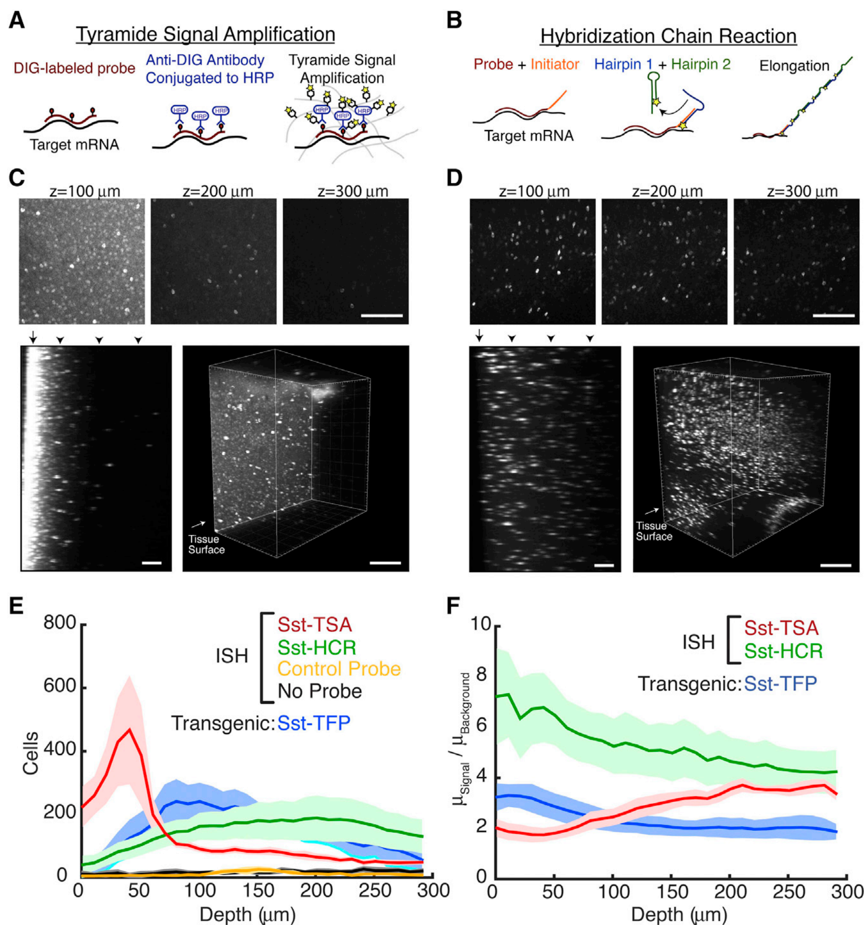

Figure 3. Comparison of Antibody-Based and DNA-Based Amplification

(A) Workflow for TSA reaction. DIG-labeled probes are hybridized to target mRNA. HRP conjugated anti-DIG antibodies bind to hybridized probes and are detected by TSA.

(B) Workflow for HCR reaction. Initiator-labeled probes are hybridized to target mRNA. In a second step, initiator sequences hybridize to toehold of fluorophore bearing hairpins, starting a chain reaction of hairpin assembly.

(C and D) In situ hybridization for *somatostatin* (Sst) mRNA in CLARITY tissue. Above, z = 100 μm, 200 μm, and 300 μm into CLARITY tissue volume of mouse cortex using traditional ISH (C) or hybridization chain reaction (D). Scale bars, 100 μm. Below, yz-subsections of CLARITY volume and 3D rendering of 1 mm sections. Arrowheads indicate the z location of the sections above. Arrows indicate the tissue surface. Due to high surface background, the top 130 μm of tissue are not shown for the 3D rendering in (C). Scale bars, 50 μm (left), 200 μm (right).

(C) DIG-labeled oligonucleotide probes detected with anti-DIG antibody (2 days) and TSA. *Somatostatin* expressing cells can be detected, but surface has high background and signal diminishes deeper in the tissue.

(D) Initiator-labeled oligonucleotide is detected with HCR reaction (1 day), resulting in more uniform staining.

(E) Number of cells as a function of tissue depth after local thresholding and cell segmentation on each imaging plane, 10 μm z interval. High surface background in TSA reaction yields a large number of putative false positives 0–75 μm into the tissue section. Detection with HCR amplification shows a more uniform labeling of cells, comparable to the distribution of *somatostatin* cells in a genetically encoded reporter mouse (Sst-TFP).

(F) Ratio of signal to background as a function of depth in tissue, calculated from ratio of mean signal intensities segmented in (F) to the mean background intensity. For (E) and (F), No Probe, n = 3; Control Probe, n = 3; TSA, n = 5; HCR, n = 9; Sst-TFP, n = 4. $p < 0.05$, Kruskal-Wallis test on mean ratio over entire depth. All error bars indicate SEM.

See also Figure S2.

We hypothesized that the main sources of surface staining and signal heterogeneity resulted from a concentration gradient of antibody penetrating the EDC-CLARITY hydrogel and consequently greater surface deposition of fluorophore during enzymatic amplification. We and others have found that probes can be labeled directly with fluorophore when RNA copy number is high and little amplification needed (Yang et al., 2014), though with limitations on sensitivity and volume size (up to 1 mm blocks, still far greater than the 20–40 μm queried with traditional techniques). Nevertheless, this restriction in volume, the need for exclusion of superficial tissue, and the severe limitation to highly expressed transcripts together pointed to the need for further innovation to exploit the speed of DNA penetration into EDC-CLARITY tissue.

DNA-Based ISH Signal Amplification

We hypothesized that an all-DNA-based amplification system rather than the traditional antibody approach might be an ideal solution. Recent work has capitalized upon the programmable base pairing of DNA molecules to design DNA structures that amplify signal by several orders of magnitude (Battich et al., 2013; Choi et al., 2010). We explored integrating this approach with EDC-CLARITY tissue chemistry, selecting the hairpin chain reaction amplification system (HCR; Choi et al., 2010) for further development since HCR (1) involves only small DNA oligonucleotides (<150 bases), which self-assemble at the target mRNA, and (2) requires only two hybridization steps (Figure 3B).

In the first hybridization step, an oligonucleotide probe containing a 36-base initiator sequence binds to target mRNA. In a second step, two fluorophore-tagged oligonucleotides are added, which are kinetically trapped in a hairpin conformation in the absence of the initiator sequence. As they diffuse into the tissue and encounter initiator sequences on hybridized probes, base pairing between the initiator sequences and the single-stranded toehold on Hairpin 1 open the hairpin, revealing a new initiator sequence capable of opening Hairpin 2. In turn, Hairpin 2 opens to reveal the original initiator sequence, starting the cycle anew. As the chain self-assembles, fluorophores

accumulate at the target location. It is estimated that the hairpin chain reaction can amplify the signal approximately 200-fold (Choi et al., 2014), and we expected that this degree of amplification might be sufficient to detect RNA in EDC-CLARITY.

To test this approach, we appended initiator sequences to the 3′ and 5′ ends of the three *somatostatin* oligonucleotide probes used above, hybridized the probes to EDC-CLARITY tissue, and amplified with HCR hairpins. We found that the combination of EDC-CLARITY and HCR amplification exhibited excellent signal, low background, produced no non-specific surface staining, and significantly improved the depth at which we could identify individual cells (Figure 3D). The signal-to-background ratio was significantly higher than in TSA-based amplification (Figure 3F) with the characteristic sparse pattern of *somatostatin* mRNA expression clearly distinguishable from background (Figure 3D). Moreover, the distribution and cell density detected with HCR amplification mirrors *somatostatin* expression in transgenic reporter mice, underscoring the specificity of this method (Sst-TFP, Figure 3E).

In Situ Hybridization in Intact Tissue

Linking information on cellular morphology, connectivity, and activity to information on RNA expression will be of substantial value; accordingly, we sought conditions for in situ hybridization in EDC-CLARITY that maintained fluorescence of transgenically expressed proteins. As a proof of concept, we performed in situ hybridization for *YFP* mRNA on Thy1-YFP transgenic mouse tissue and formulated a hybridization buffer that allowed reduction of hybridization temperature from 45°C to 37°C, which improved fluorescence in dendrites and axons while maintaining ISH specificity (Figures 4A and S2 and Movie S1). To provide a generalizable framework for HCR-based RNA detection in EDC-CLARITY, we used these hybridization conditions to design, test, and refine sets of 50-mer DNA probes for several representative and broadly useful target RNAs for molecular phenotyping in nervous system tissue: *somatostatin*, *parvalbumin*, *neuropeptide Y* (*NPY*), *vasoactive intestinal peptide* (*VIP*), *tachykinin1*, *tachykinin2*, *tyrosine hydroxylase*, and *Malat1*. These targets showed reliable signal in EDC-CLARITY tissue and corresponded to known anatomical distributions in both neural and non-neural tissue (Figures 4B–4I and Figure S3).

In refining these probe sets, we typically performed initial testing on pools of 5–10 probes; in cases where we observed non-specific staining, we then tested probes individually to identify and discard probes contributing significantly to background, which improved image quality (Figure S4A). Under these conditions, we estimate that HCR in CLARITY tissue results in ~50-fold amplification per double-initiator-labeled probe (Figures S4D–S4F). In agreement with previous results, increasing the number of initiators, whether by adding initiators to both 5′ and 3′ ends or by adding more probes, enhances signal substantially (Choi et al., 2014). This effect may eventually saturate if limited by slightly sublinear amplification (Figures S4B and S4C), but low copy-number transcripts may still benefit from a larger set of probes. In comparing these results to published data from single-cell transcriptomics (Zeisel et al., 2015), we find that our data capture relative differences among gene expression levels across almost 2 orders of magnitude (Figures S4G and S4H); indeed, with 4 probes per target, this approach allows detection of mRNAs present at as low as ~50 copies/cell (Figure S4H). Although not as sensitive as RNA-seq, probe sets can be expanded as shown below, and the large volumes processed in a single CLARITY experiment enable inclusion of spatial information and sampling from many more cells than would be achieved with RNA-seq (particularly important if genes are expressed in sparse subsets within a tissue).

Since low copy-number transcripts may benefit from additional probes and since it was important to determine if our methodology could be readily adapted to diverse probe design strategies, we tested the feasibility of using a larger set of shorter probes by attaching initiators to the 5′ end of probe sets originally designed for single-molecule fluorescent in situ hybridization (smFISH), which typically uses 20-mer oligonucleotides (30–50 probes) that tile the mRNA target sequence. As with directly fluorophore-labeled 20-mer probes, we expected that with many HCR-labeled 20-mers, the on-target signal would accumulate in cells in which many probes bind and amplify (whereas off-target binding would be uniform across the sample); we did not, however, expect that HCR with these probes would provide single-molecule capability. Using this strategy, we were able to detect *tyrosine hydroxylase*, *SERT*, and *Drd2* mRNA in EDC-CLARITY tissue, demonstrating that the HCR approach is adaptable to other probe types in CLARITY and compatible with larger pools of short probes (Figures 4J–4L and Movies S2 and S3). Because longer nucleotides are more expensive to synthesize and purify, the strategy of using short probes would reduce overall cost and may enable significantly greater signal amplification.

Likely owing to the quick and uniform diffusion of DNA probes and hairpins, we find that tissue blocks up to at least 3 mm thick could be used for intact in situ hybridization (Figure 4M and Movies S4 and S5). Another unique advantage of nucleic acid detection (relative to antibody-based detection) is that once the target sequence is known, it is possible to design probes for the target that are highly specific, permanently renewable, and cost effective. We therefore anticipate that this methodology for RNA detection in EDC-CLARITY may be versatile for probing a variety of transcriptional products across many tissue-types and species.

Detection of Activity-Dependent Genes and Non-coding RNAs in Intact Volumes

Many mRNAs are transiently upregulated by activity, a fact that has been instrumental in identifying cells and circuits recruited during particular behaviors (e.g., Loebrich and Nedivi, 2009). Using such immediate early genes (IEGs), it has been possible to identify neurons involved in complex behaviors (even multiple behaviors separated in time; Guzowski et al., 1999; Reijmers et al., 2007), to visualize behaviorally relevant neurons in transgenic mice, in some cases long after the behavior itself (Barth et al., 2004; Guenthner et al., 2013; Smeyne et al., 1992), and to manipulate these IEG-expressing neurons to modify or recapitulate the observed behavior (Garner et al., 2012; Liu et al., 2012; Ramirez et al., 2013). Yet a major unmet goal is linking form and function: to align these transcriptional activity changes with molecular phenotype and connectivity information in large intact volumes. We therefore next designed HCR probe sets against several canonical activity-regulated transcripts, *Arc*

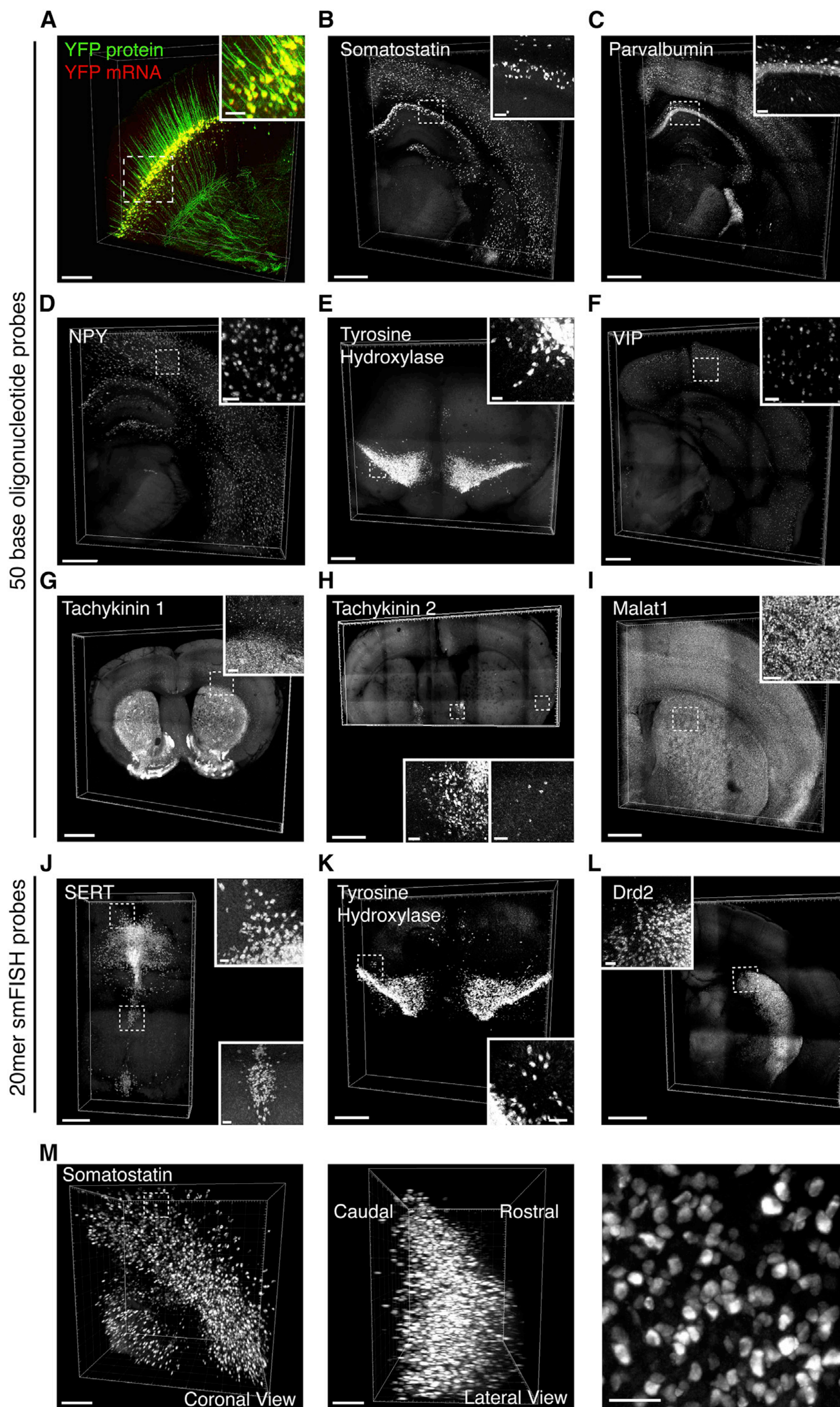

Figure 4. Cell-Type Phenotyping in CLARITY Tissue Using DNA Probes and HCR Amplification

(A) 3D rendering of 1-mm-thick coronal section from Thy1-YFP mouse, in situ hybridization for *YFP* mRNA in red, endogenous YFP fluorescence in green. Scale bar, 200 μm. Inset, 3D rendering of boxed section in cortex. Scale bar, 50 μm.

(B–L) 3D rendering of in situ hybridization performed in 0.5 mm coronal CLARITY sections using 50-mer DNA oligonucleotide probes. Scale bars, 500 μm; insets, 50 μm, unless otherwise noted.

(B) *Somatostatin* mRNA (four probes).

(C) *Parvalbumin* mRNA (four probes). Inset scale bar, 70 μm.

(D) *Neuropeptide* Y mRNA (five probes).

(E) *Tyrosine hydroxylase* mRNA (ten probes).

(F) *Vasoactive Intestinal Peptide* (VIP) mRNA (five probes).

(G) *Tachykinin1* mRNA (five probes). Scale bar, 1 mm; inset, 100 μm.

(H) *Tachykinin2* mRNA (four probes). Scale bar, 1000 μm; inset of BNST and cortex, 50 μm.

(I) *Malat1* mRNA (four probes).

(J–L) 3D rendering of in situ hybridization performed in 0.5 mm CLARITY sections using 20-mer DNA oligonucleotides.

(J) *SERT* mRNA (47 probes).

(K) *Tyrosine hydroxylase* mRNA (39 probes).

(L) *Drd2* mRNA (39 probes). Scale bar, 1,500 μm; inset, 50 μm.

(M) Left, 3D rendering of 2 mm block of mouse cortex, processed with EDC-CLARITY with in situ hybridization for *somatostatin* using HCR amplification. Middle: orthogonal view of volume at left, showing signal throughout tissue depth. Scale bars, 200 μm. Right: magnified view of *somatostatin*-expressing cells in cortex from volume at left. Scale bar, 50 μm.

See also Figures S3 and S4.

(Lyford et al., 1995), *c-fos* (Sheng et al., 1990), and *Npas4* (Bloodgood et al., 2013), and tested these probes in a kainic acid seizure model (known to induce robust hippocampal transcription of many activity-regulated genes; Nedivi et al., 1993). We found that we were able to reliably track changes in expression of all of these activity-regulated genes in EDC-CLARITY. For example, *Npas4* is normally expressed in scattered cells in cortex but is robustly transcribed in both hippocampal pyramidal cells and interneurons after seizure activity (Figure 5A). In parallel experiments, increases in *c-Fos* transcription in hilar neurons and *Arc* transcription in dentate granule cells were readily detectable (Figures 5B and 5C), as described previously in hippocampal seizure models (Lyford et al., 1995).

Lastly, we assessed detection of small-noncoding RNAs—a major motivation for this entire approach since these are undetectable by antibodies yet also are (1) critical for the modulation of post-transcriptional gene expression; (2) play key roles in human genetic diseases (Esteller, 2011); and(3) represent a wealth of biological information not yet approached by any tissue clearing technique. Indeed, due to small size, microRNAs have fewer amines to react with paraformaldehyde or acrylamide and are easily lost from fixed tissues (Pena et al., 2009; Renwick et al., 2013).

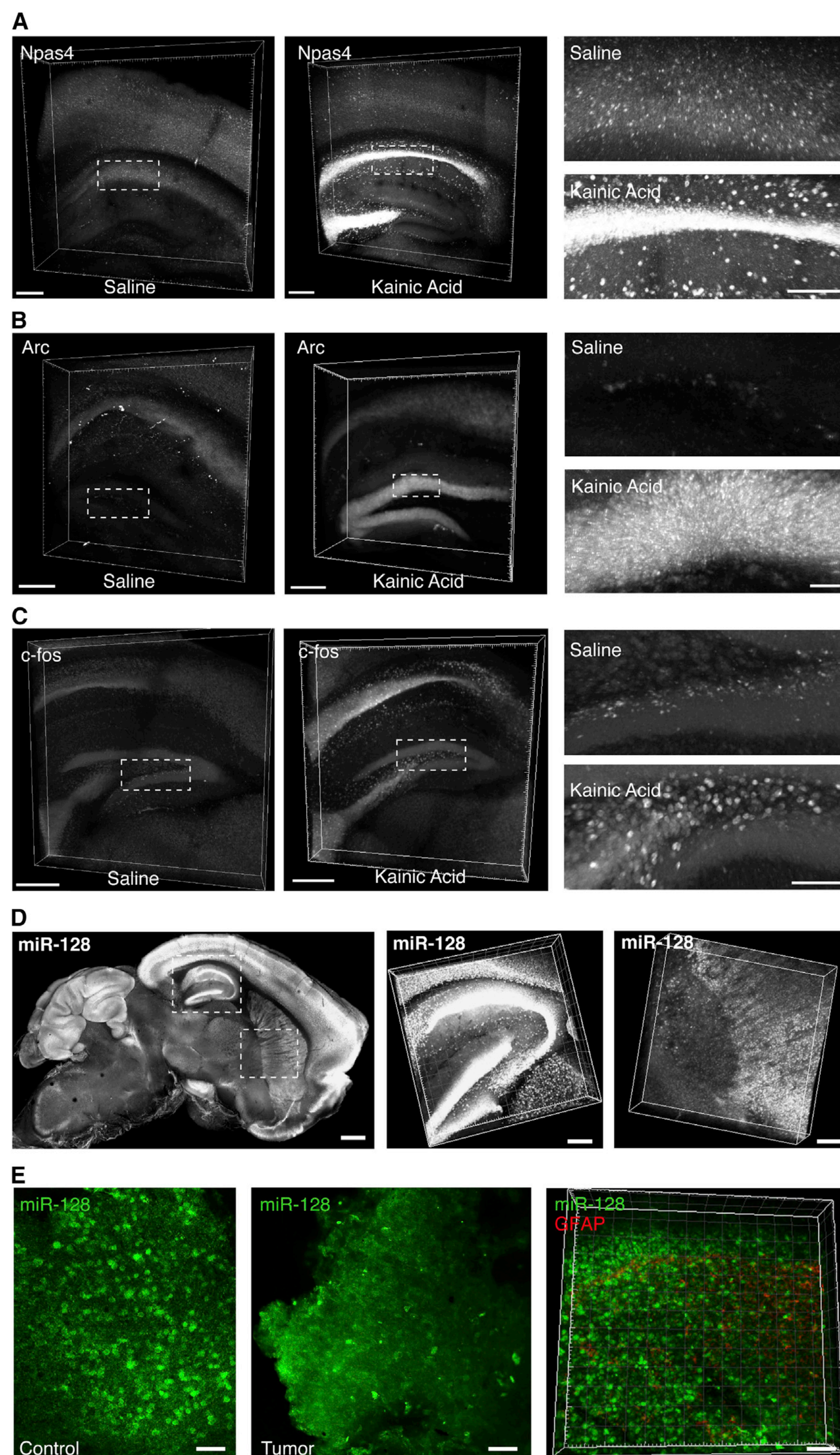

Figure 5. Detecting Activity-Induced Transcripts and Non-coding RNAs in CLARITY Volumes

(A–C) 3D rendering of 0.5 mm CLARITY section, HCR in situ hybridization in control saline injected (left) and kainic acid injected (right) animals. Kainic acid, 12 mg/kg, i.p., 2 hr prior to perfusion.

(A) *Npas4* mRNA (four probes). Scale bar, 200 μm. Right, magnified view of indicated boxes. Scale bar, 100 μm.

(B) *Arc* mRNA (five probes). Right, magnified view of indicated boxes. Scale bar, 50 μm.

(C) *c-fos* mRNA (45 probes). Scale bars, 500 μm; Right, magnified view of dentate gyrus as indicated by dotted box. Scale bar, 100 μm.

(D) Left, projection image of 1 mm mouse brain sagittal section, cleared, and hybridized with DIG-labeled LNA probes for mature *miR-128* sequence. Scale bar, 500 μm. Middle, right 10× zoom of hippocampal and striatal volumes respectively. Scale bar, 150 μm.

(E) Left, projection images of human brain control (left) and tumor (GBM) (middle) samples, cleared and in situ hybridized for *miR-128* (green). Scale, 50 μm (right). Volume reconstruction of human GBM tumor biopsy sample (200 μm thick; scale, 50 μm) also stained with antibody to GFAP (red). *miR-128* and GFAP have orthogonal signal gradients within the tumor preparation.

See also Figure S5.

Consistent with this expected challenge, we found that post-treatment with EDC was critical for the retention of miRNAs in EDC-CLARITY (Figure S5A). Using DIG-labeled locked nucleic acid probes, we targeted several miRNAs with known function in the mammalian brain and in neuropsychiatric disease (*miR-10*, *miR-124*, and *miR-128*), as well as a miRNA known to exist only outside the mammalian brain (*miR-21*) to serve as a negative control (Landgraf et al., 2007). We detected robust expression of these miRNAs in volumes of mouse brain in a pattern largely limited to areas with anticipated expression (as inferred from miRNA deep-sequencing experiments). *miR-10* signal (for instance) was almost exclusively recovered in the thalamus, *miR-124* was observed to be more ubiquitously present throughout the brain, and *miR-128* showed characteristic forebrain and cerebellar enrichment (Figures 5D, S5B, and S5C). We observed minimal signal for *miR-21* under the same detection and amplification conditions, as expected, highlighting the specificity of the miRNA signals observed (Figures S5B and S5C).

miR-128 is particularly well studied in the context of its known disease-relevance for oncogenic suppression (Pang et al., 2009) and predisposition to mood disorders (Zhou et al., 2009), but until now, *miR-128* expression has not been visualized volumetrically in the mammalian brain at single-cell resolution, which we were readily able to achieve here (Figure 5D). To further test potential utility of this approach in the study of brain disease, we endeavored to detect *miR-128* in

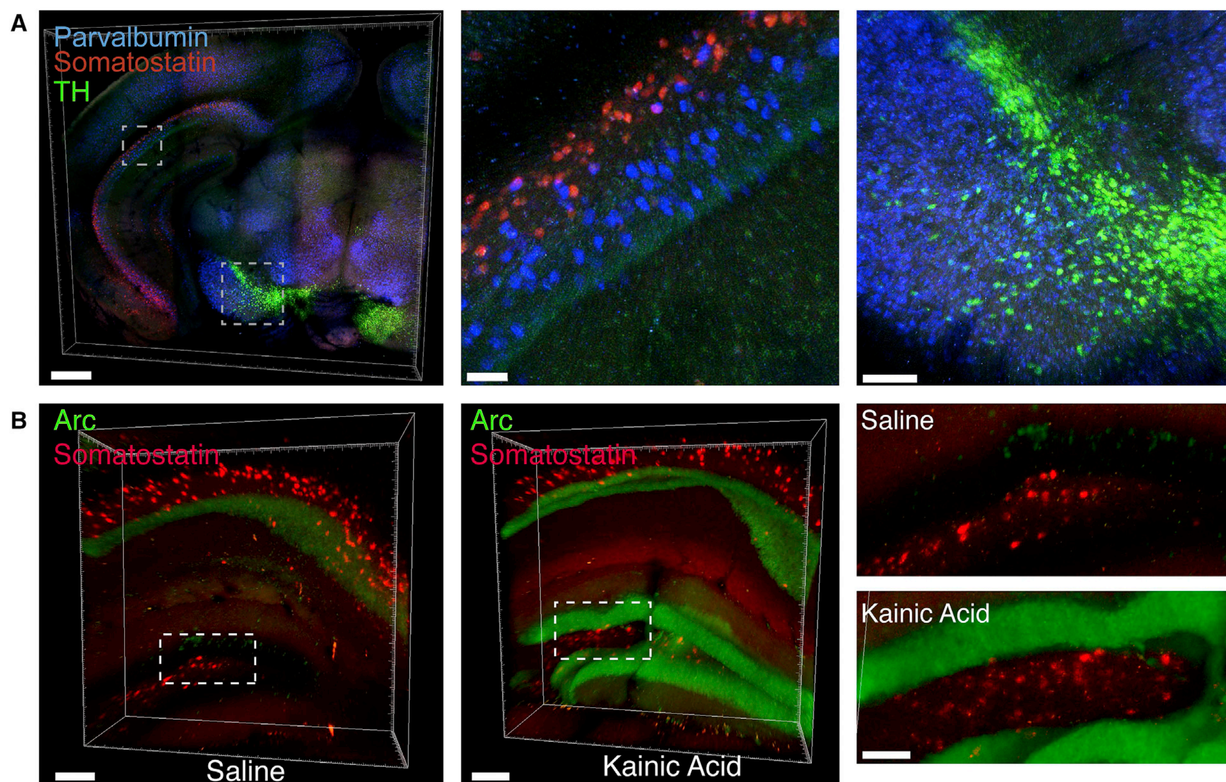

Figure 6. Multiplexed Detection of mRNAs in CLARITY

(A) Left, multiplexed in situ hybridization of 0.5 mm coronal CLARITY section treated with kainic acid, using *somatostatin* (red), *parvalbumin* (blue), and *tyrosine hydroxylase* (green) probe sets. Scale bar, 500 μm. Middle, inset of caudal hippocampus showing *parvalbumin* and *somatostatin* interneurons in CA1 region. Scale bar, 50 μm. Right, *parvalbumin* and *tyrosine hydroxylase* positive cells in midbrain. Scale bar, 100 μm.

(B) 3D rendering of 1 mm CLARITY block, HCR in situ hybridization for *somatostatin* (red) and *Arc* mRNA (green) in control saline injected (left) and kainic acid injected (right) animals. Right, magnified view of indicated boxes. Scale bar, 100 μm.

See also Figure S6.

human clinical samples to determine if differences in expression might be associated with human glioblastomas (suggested but not directly observed; Ciafrè et al., 2005). We indeed were able to detect *miR-128* in human GBM samples processed in EDC-CLARITY hydrogel; moreover, by integrating antibody staining (in this case, GFAP to mark tumor location) with ISH in EDC-CLARITY, we could track the crucial relative relationships of GFAP and *miR-128* expression across the tissue volume at cellular resolution (Figure 5E). Such an approach designed to provide 3D volumetric access to miRNAs in biopsied or post-mortem human brain samples may be valuable in the search for tissue-level disease insights, biomarkers, and therapeutic targets for neurological and psychiatric disease.

Multiplexed Molecular Phenotyping

Finally, we sought to develop methods for multiplexed detection of RNA in EDC-CLARITY to address the critical and rapidly growing need for multiple overlaid markers of cell identity or activity in the native anatomical context. Using multiplexed hybridization and amplification with orthogonal hairpin sets (Choi et al., 2014), we were able to simultaneously label multiple mRNAs in EDC-CLARITY. Of note, although orthogonal hairpins were equivalent in amplification, individual fluorophores varied in fluorescence signal, as may be expected by differences in tissue autofluorescence, fluorophore efficiency, and light transmittance at different wavelengths (Figure S6). Nevertheless, *somatostatin*, *parvalbumin*, and *tyrosine hydroxylase* could be simultaneously hybridized and amplified with sets of orthogonal hairpins carrying Alexa514, Alexa647, and Alexa546 fluorophores, respectively (Figure 6A and Movie S5). We were also able to combine in situ hybridization for cell-type markers with in situ hybridization for activity markers (Figure 6B). Taken together, these data demonstrate key steps toward integrated investigation of cellular structure and typology, microRNA expression, and activity-regulated gene transcription within intact tissue volumes.

DISCUSSION

While whole-mount in situ hybridization has long been a standard technique to query RNA populations in small transparent or embryonic tissue, the scattering properties of adult tissues have prevented extension to most adult samples. Moreover, while tissue clearing methods to meet the challenge of scattering have been described for over 100 years (Spalteholz, 1911), along

with a resurgence in interest and innovation over the past decade, visualization of RNA in large blocks of intact tissue has remained largely unaddressed (Richardson and Lichtman, 2015) despite significant advantages over protein labeling for reasons discussed above (briefly: scaling, cost, renewability, availability for all transcripts, consistency across preparations, and inclusivity of nontranslated mRNAs). Here, we report development of general methodology, tools, and resources for cellular-resolution transcriptional profiling of large and intact transparent mammalian tissue volumes, with reliable detection of diverse markers for non-coding transcripts, cell identity, and activity history.

Critically, while hydrophobic solvent- and immersion-based techniques have emerged as methods for clearing and immunostaining tissue, none have demonstrated successful RNA detection. Although these techniques might be optimized in this direction, key components could be incompatible with RNA detection. For example, in ClearT2 (an immersion-based method) the use of formamide during clearing (which is also used during hybridization to destabilize RNA duplexes) may pose challenges for probe hybridization (Kuwajima et al., 2013). Likewise, ScaleA2, ScaleU2, ScaleS, and CUBIC use urea (Hama et al., 2011; 2015; Susaki et al., 2014; Tainaka et al., 2014), also a destabilizing agent for hybridization (Simard et al., 2001). Finally, hydrophobic solvent-based clearing methods (such as the 3DISCO and iDISCO techniques; Ertürk et al., 2012; Renier et al., 2014) crosslink tissue with methanol prior to solvent clearing, which may limit access to RNA for hybridization in large volumes, and indeed, RNA labeling has not yet been shown in any of these volumetric methods. Since the specificity of nucleic acid probe hybridization requires maintenance of specific concentrations of salt and organic solvent (such as formamide) in a window that favors probe hybridization to target but not off-target RNA, aqueous-based CLARITY/hydrogel approaches appear to provide unique RNA detection advantages for compatibility with commonly used hybridization reagents.

Almost all in situ hybridization techniques for fixed tissue require permeabilization prior to hybridization to enable access of probes to target RNA (Wilkinson, 1999). Intrinsic to the CLARITY process is permeabilization of tissue via removal of lipid membranes and denaturation of proteins, enabling RNA access without necessity of proteases (though proteases may be used as well in some forms of CLARITY). Without stabilization via cross-linking, RNA is susceptible to rapid degradation by endogenous RNases; in EDC-CLARITY, RNA is stabilized by both PFA cross-linking (which fixes RNA and renders RNases immobile) and EDC. Together, these properties may make EDC-CLARITY particularly suitable for RNA detection; nevertheless, the methodologies we describe might also be suitable for hybrid approaches to volumetric RNA detection in other clearing methods, given sufficient optimization of fixation and permeabilization parameters.

We have presented validation for select microRNAs, cell-type markers, and immediate-early genes, but with the RNA landscape preserved via EDC fixation, we anticipate that this method could be extended to additional RNA species. Oligonucleotide or LNA probes could be designed for splice junctions to visualize brain-wide expression of particular mRNA variants. Because CLARITY tissue maintains subcellular structures, this method also dovetails with catFISH approaches, where nuclear localization (or intronic or exonic targeting probes) could be used to temporally differentiate two activity-triggered transcriptional events (Guzowski et al., 1999; Lin et al., 2011). The ability in EDC-CLARITY to use a variety of different probe types (50-mer oligos, 20-mer oligos, LNAs) and amplification methods (HCR for multiplexing and larger volumes, TSA for smaller volumes) suggests versatility, but as always, in situ hybridization must be further tailored to RNA target type, volume size, copy number, transcript length, and species.

The ability to monitor many transcripts simultaneously will be of growing relevance as the field moves toward increasingly rich and detailed molecular phenotyping. For HCR amplification, there are currently five validated hairpin sets allowing up to five targets to be labeled simultaneously (Choi et al., 2014), but spectral separation will be a limiting factor in expanding these further. The sharp emission spectra of quantum dots could address this problem, though the effect of steric hindrance on hairpin assembly and diffusion of oligonucleotides will require testing. Opportunities associated with multi-feature typology extend beyond multiple molecular features, and include fusing molecular and anatomical datasets. Whereas typical in situ protocols degrade fluorescence, the approach shown here is compatible with maintained fluorescence of genetically encoded cell-filling proteins for visualization of 3D neuronal morphology and wiring (and thus allows integration of information about molecular identity and functional history with information on local and global connectivity across intact nervous systems).

The goal of identifying low-copy-number transcripts can be approached from several angles. During amplification, initiators could be concatenated or combined with a branched DNA approach (Battich et al., 2013) to incorporate more initiator sequences onto each probe. Additional fluorophores, or photobleach-resistant quantum dots, could be conjugated to hairpins to improve signal (Resch-Genger et al., 2008). During hybridization, we have demonstrated that 20-mer probes could be used to tile the entire sequence with initiators, which would be particularly effective in improving detection for rare, but long transcripts. Alternatively, one could directly reverse-transcribe mRNA and amplify the resulting cDNA in situ (successful for in situ sequencing strategies), though hydrogel properties may require optimization for best enzymatic activity and diffusion of key components (Ke et al., 2013; Lee et al., 2014).

Having characterized in EDC-CLARITY an array of probe sets for canonical markers of cell identity and activity, to facilitate the community's further benefit from (and engagement with) this growing effort of probe testing and publication, we have established a database of validated probes, with sequences and hybridization conditions available as an open online resource (http://clarityresourcecenter.org, http://wiki.claritytechniques.org/index.php/ISH). Requiring little specialized equipment, low startup costs, and moderate operational costs, this approach could provide an alternative to immunohistochemistry when specific antibodies are lacking or to traditional in situ hybridization and serial sectioning when streamlined data acquisition is needed, as with large cohorts or large tissue volumes. While each step will benefit from further innovation and optimization,

flexible design of EDC-CLARITY methodologies may favor adoption across a broad application domain, from clinical samples to integrative basic analysis of structure-function properties spanning cell typology, activity in behavior, and local and global tissue relationships.

EXPERIMENTAL PROCEDURES

CLARITY Tissue Preparation

CLARITY tissue was prepared as described in Tomer et al. (2014). For A4P0 samples, tissues were prepared as described in Yang et al. (2014). Tissue was incubated with RNA fixatives after acrylamide polymerization (EDC, 0.1 M; PMPI, 0.1 M; or DSS, 0.1 M, overnight at 37°C). Tissue was cleared passively in a 4% SDS/ 0.2 M Boric acid (pH = 8.5) clearing solution at 37°C until transparent and stored in 1× PBS with 0.3% TX-100 (PBST) at 4°C.

Total RNA Isolation and Acridine Orange Staining

Cleared tissue was homogenized in 20 μg/ml proteinase K and extracted with Trizol and then acidic phenol:chloroform:isoamyl alcohol before precipitation with ethanol. For acridine orange staining, sections were rinsed in sodium citrate (SC) buffer for 10 min, incubated in acridine orange solution (100 μg/ml) for 3 hr, then rinsed in SC buffer and then PBS, and transferred to refractive index matching in FocusClear.

Probe Design

Riboprobes were generated from cDNA templates, reverse transcribed with DIG-labeled dNTPs (Roche), and purified. smFISH probes were designed and synthesized by BioSearch. DNA 50-mer oligonucleotide probes were purchased from Molecular Instruments (Caltech) or designed using OligoWiz software (Wernersson et al., 2007) and synthesized by Integrated DNA Technologies. LNA probes were synthesized by Exiqon.

Probe and Antibody Diffusion

For RNA and DNA probe diffusion, cleared tissue (2 mm) was incubated in hybridization solution for the time indicated, then cooled to 4°C, fixed with PFA, and re-sectioned (200 μm). Cross-sections of the center of tissue were selected for staining with anti-DIG antibody conjugated to HRP and detected with TSA.

For antibody diffusion, tissue was incubated in 50-mer DIG-labeled oligonucleotides overnight in 40% formamide and 2×SSC, cooled to 4°C, and fixed in 4% PFA for 1 hr at RT. The tissue was then incubated with anti-DIG Fab fragment antibody coupled to HRP (1:500) in PBST for the corresponding time and further processed as above for re-sectioning and TSA amplification.

In Situ Hybridization

For all in situ hybridizations, cleared tissue was equilibrated in hybridization solution for 1 hr and hybridized in the same solution overnight at 37°C unless otherwise noted, and then stringency washes were performed at the hybridization temperature to remove excess or non-specifically bound probe. Solutions and temperatures varied for each probe type and are as follows. Oligo(dT): hybridization with 15% formamide, 2xSSC, 10% dextran sulfate, 50 nM probe; stringency 3× 1 hr in 15% formamide, 2×SSC then 2× 1 hr in 2×SSC. DIG-labeled 50-mers: hybridization with 50% formamide, 5×SSC, 0.5 mg/ml yeast tRNA; stringency 3× 1 hr in 50% formamide, 5×SSC plus 2× 1 hr in 2×SSC and then transferred to PBST. Initiator-labeled 50-mers: hybridization with 40% formamide, 2×SSC, 10% dextran sulfate, 0.5 mg/ml yeast tRNA; stringency 3×1 hr in 40% formamide, 2×SSC plus 2×1 hr in 2×SSC. DNA 20-mers (smFISH sets): hybridization with 10% formamide, 2×SSC, 10% dextran sulfate; stringency 3×1 hr in 10% formamide, 2×SSC plus 2×1 hr in 2×SSC. LNA probes: hybridization with 50% formamide, 5×SSC, 0.5 mg/ml yeast tRNA, 12.5 nM DIG-labeled probe at 20°C below Tm; stringency 2×1 hr in 5×SSC plus 1 hr in 2×SSC at the same temperature.

For DIG-labeled probes, tissue was washed in PBST after stringency. Tissue was incubated overnight in anti-DIG antibody conjugated to HRP (1:500) for 2 days per mm tissue thickness, washed overnight in PBST, developed with tyramide signal amplification (1:50 dilution, 30 min), washed 3× in PBST, and transferred to FocusClear for imaging. For initiator probes, tissue was equilibrated in amplification buffer (5×SSC, 0.1% Tween20, 10% dextran sulfate). DNA hairpins were separately heated to 90°C, cooled to RT, and added to amplification buffer. Tissue was incubated in hairpins overnight at RT, then washed 5× 1 hr with 5×SSC plus 0.1% Tween20, and transferred to FocusClear for imaging.

Propidium iodine staining, where applicable, was performed using a PropI/RNase solution after stringency washes. Sections were transferred to FocusClear for 4 hr prior to imaging. Tissue shrinks once equilibrated to FocusClear for imaging; all scale bars represent the imaged volume, which is ~50% of original tissue volume.

Human Tissue

Human tissue is putative healthy tissue obtained from temporal lobe resections from two patients (46-year-old female, 18-year-old male). Tissue was equilibrated in 1% hydrogel solution for 2 days at 4°C, polymerized for 5 hr at 37°C, and cleared for 5 weeks in 4% SDS at 37°C.

Confocal Microscopy

All images were taken on a Leica SP5 confocal microscope with a 10×/0.4 objective (WD: 2.2 mm) or 20×/0.75 objective (WD: 0.66 mm) at 488 nm (FITC), 514 nm, 543 nm, or 647 nm excitation.

Experimental Subjects

Animal husbandry and all aspects of animal care and euthanasia as described were in accordance with guidelines from the NIH and have been approved by members of the Stanford Institutional Animal Care and Use Committee. Use of surgical and post-mortem human tissue was in accordance with guidelines from the NIH and approved by the Stanford Institutional Review Board.

SUPPLEMENTAL INFORMATION

Supplemental Information includes Supplemental Experimental Procedures, six figures, one table, and five movies and can be found with this article online at http://dx.doi.org/10.1016/j.cell.2016.01.038.

AUTHOR CONTRIBUTIONS

E.L.S., P.R., M.A.W., and K.D. designed experiments; P.R. and A.J. developed and characterized fixation conditions, designed and implemented microRNA in situ hybridization experiments, and analyzed data; E.L.S. and M.A.W. characterized diffusion conditions, designed and implemented mRNA in situ hybridization experiments, and analyzed data; E.L.S., P.R., M.A.W., and K.D. wrote the paper; and K.D. supervised all aspects of the work.

ACKNOWLEDGMENTS

We thank Niles Pierce and Harry Choi for generously making HCR reagents freely available and for advice during protocol troubleshooting. We thank Michelle Monje for providing human glioblastoma tumor samples and the entire Deisseroth lab for helpful discussions. This work is supported by an Ellison LSRF fellowship (P.R.), NIH T32 Fellowship (M.A.W.), and NIMH, NIDA, and the U.S. Army Research Laboratory and Defense Advanced Research Projects Agency (Cooperative Agreement Number W911NF-14-2-0013); nothing in this material represents official views or policies of our funders. K.D. is a founder and scientific advisor of ClearLight Diagnostics, a startup exploring improvement of cancer diagnostics using CLARITY-related methods; the authors have disclosed these findings to the Stanford Office of Technology Licensing, and all clones, sequences, protocols and resources are freely distributed and supported (http://clarityresourcecenter.org and http://wiki.claritytechniques.org/index.php/ISH).

Received: October 4, 2015
Revised: December 28, 2015
Accepted: January 25, 2016
Published: February 11, 2016

REFERENCES

Barth, A.L., Gerkin, R.C., and Dean, K.L. (2004). Alteration of neuronal firing properties after in vivo experience in a FosGFP transgenic mouse. J. Neurosci. *24*, 6466–6475.

Battich, N., Stoeger, T., and Pelkmans, L. (2013). Image-based transcriptomics in thousands of single human cells at single-molecule resolution. Nat. Methods *10*, 1127–1133.

Bloodgood, B.L., Sharma, N., Browne, H.A., Trepman, A.Z., and Greenberg, M.E. (2013). The activity-dependent transcription factor NPAS4 regulates domain-specific inhibition. Nature *503*, 121–125.

Choi, H.M.T., Chang, J.Y., Trinh, A., Padilla, J.E., Fraser, S.E., and Pierce, N.A. (2010). Programmable in situ amplification for multiplexed imaging of mRNA expression. Nat. Biotechnol. *28*, 1208–1212.

Choi, H.M.T., Beck, V.A., and Pierce, N.A. (2014). Next-generation in situ hybridization chain reaction: higher gain, lower cost, greater durability. ACS Nano *8*, 4284–4294.

Chung, K., Wallace, J., Kim, S.-Y., Kalyanasundaram, S., Andalman, A.S., Davidson, T.J., Mirzabekov, J.J., Zalocusky, K.A., Mattis, J., Denisin, A.K., et al. (2013). Structural and molecular interrogation of intact biological systems. Nature *497*, 332–337.

Ciafrè, S.A., Galardi, S., Mangiola, A., Ferracin, M., Liu, C.-G., Sabatino, G., Negrini, M., Maira, G., Croce, C.M., and Farace, M.G. (2005). Extensive modulation of a set of microRNAs in primary glioblastoma. Biochem. Biophys. Res. Commun. *334*, 1351–1358.

Denk, W., and Horstmann, H. (2004). Serial block-face scanning electron microscopy to reconstruct three-dimensional tissue nanostructure. PLoS Biol. *2*, e329.

Dodt, H.-U., Leischner, U., Schierloh, A., Jährling, N., Mauch, C.P., Deininger, K., Deussing, J.M., Eder, M., Zieglgänsberger, W., and Becker, K. (2007). Ultramicroscopy: three-dimensional visualization of neuronal networks in the whole mouse brain. Nat. Methods *4*, 331–336.

Ertürk, A., Becker, K., Jährling, N., Mauch, C.P., Hojer, C.D., Egen, J.G., Hellal, F., Bradke, F., Sheng, M., and Dodt, H.-U. (2012). Three-dimensional imaging of solvent-cleared organs using 3DISCO. Nat. Protoc. *7*, 1983–1995.

Esteller, M. (2011). Non-coding RNAs in human disease. Nat. Rev. Genet. *12*, 861–874.

Garner, A.R., Rowland, D.C., Hwang, S.Y., Baumgaertel, K., Roth, B.L., Kentros, C., and Mayford, M. (2012). Generation of a synthetic memory trace. Science *335*, 1513–1516.

Guenthner, C.J., Miyamichi, K., Yang, H.H., Heller, H.C., and Luo, L. (2013). Permanent genetic access to transiently active neurons via TRAP: targeted recombination in active populations. Neuron *78*, 773–784.

Guzowski, J.F., McNaughton, B.L., Barnes, C.A., and Worley, P.F. (1999). Environment-specific expression of the immediate-early gene Arc in hippocampal neuronal ensembles. Nat. Neurosci. *2*, 1120–1124.

Hama, H., Kurokawa, H., Kawano, H., Ando, R., Shimogori, T., Noda, H., Fukami, K., Sakaue-Sawano, A., and Miyawaki, A. (2011). Scale: a chemical approach for fluorescence imaging and reconstruction of transparent mouse brain. Nat. Neurosci. *14*, 1481–1488.

Hama, H., Hioki, H., Namiki, K., Hoshida, T., Kurokawa, H., Ishidate, F., Kaneko, T., Akagi, T., Saito, T., Saido, T., and Miyawaki, A. (2015). ScaleS: an optical clearing palette for biological imaging. Nat. Neurosci. *18*, 1518–1529.

Ke, R., Mignardi, M., Pacureanu, A., Svedlund, J., Botling, J., Wählby, C., and Nilsson, M. (2013). In situ sequencing for RNA analysis in preserved tissue and cells. Nat. Methods *10*, 857–860.

Kuwajima, T., Sitko, A.A., Bhansali, P., Jurgens, C., Guido, W., and Mason, C. (2013). ClearT: a detergent- and solvent-free clearing method for neuronal and non-neuronal tissue. Development *140*, 1364–1368.

Landgraf, P., Rusu, M., Sheridan, R., Sewer, A., Iovino, N., Aravin, A., Pfeffer, S., Rice, A., Kamphorst, A.O., Landthaler, M., et al. (2007). A mammalian microRNA expression atlas based on small RNA library sequencing. Cell *129*, 1401–1414.

Lee, J.H., Daugharthy, E.R., Scheiman, J., Kalhor, R., Yang, J.L., Ferrante, T.C., Terry, R., Jeanty, S.S.F., Li, C., Amamoto, R., et al. (2014). Highly multiplexed subcellular RNA sequencing in situ. Science *343*, 1360–1363.

Li, J., Czajkowsky, D.M., Li, X., and Shao, Z. (2015). Fast immuno-labeling by electrophoretically driven infiltration for intact tissue imaging. Sci. Rep. *5*, 10640.

Lin, D., Boyle, M.P., Dollar, P., Lee, H., Lein, E.S., Perona, P., and Anderson, D.J. (2011). Functional identification of an aggression locus in the mouse hypothalamus. Nature *470*, 221–226.

Liu, X., Ramirez, S., Pang, P.T., Puryear, C.B., Govindarajan, A., Deisseroth, K., and Tonegawa, S. (2012). Optogenetic stimulation of a hippocampal engram activates fear memory recall. Nature *484*, 381–385.

Loebrich, S., and Nedivi, E. (2009). The function of activity-regulated genes in the nervous system. Physiol. Rev. *89*, 1079–1103.

Lyford, G.L., Yamagata, K., Kaufmann, W.E., Barnes, C.A., Sanders, L.K., Copeland, N.G., Gilbert, D.J., Jenkins, N.A., Lanahan, A.A., and Worley, P.F. (1995). Arc, a growth factor and activity-regulated gene, encodes a novel cytoskeleton-associated protein that is enriched in neuronal dendrites. Neuron *14*, 433–445.

Masuda, N., Ohnishi, T., Kawamoto, S., Monden, M., and Okubo, K. (1999). Analysis of chemical modification of RNA from formalin-fixed samples and optimization of molecular biology applications for such samples. Nucleic Acids Res. *27*, 4436–4443.

Mattson, G., Conklin, E., Desai, S., Nielander, G., Savage, M.D., and Morgensen, S. (1993). A practical approach to crosslinking. Mol. Biol. Rep. *17*, 167–183.

Micheva, K.D., and Smith, S.J. (2007). Array tomography: a new tool for imaging the molecular architecture and ultrastructure of neural circuits. Neuron *55*, 25–36.

Nedivi, E., Hevroni, D., Naot, D., Israeli, D., and Citri, Y. (1993). Numerous candidate plasticity-related genes revealed by differential cDNA cloning. Nature *363*, 718–722.

Oh, S.W., Harris, J.A., Ng, L., Winslow, B., Cain, N., Mihalas, S., Wang, Q., Lau, C., Kuan, L., Henry, A.M., et al. (2014). A mesoscale connectome of the mouse brain. Nature *508*, 207–214.

Pang, J.C.-S., Kwok, W.K., Chen, Z., and Ng, H.-K. (2009). Oncogenic role of microRNAs in brain tumors. Acta Neuropathol. *117*, 599–611.

Pena, J.T.G., Sohn-Lee, C., Rouhanifard, S.H., Ludwig, J., Hafner, M., Mihailovic, A., Lim, C., Holoch, D., Berninger, P., Zavolan, M., and Tuschl, T. (2009). miRNA in situ hybridization in formaldehyde and EDC-fixed tissues. Nat. Methods *6*, 139–141.

Ramirez, S., Liu, X., Lin, P.-A., Suh, J., Pignatelli, M., Redondo, R.L., Ryan, T.J., and Tonegawa, S. (2013). Creating a false memory in the hippocampus. Science *341*, 387–391.

Reijmers, L.G., Perkins, B.L., Matsuo, N., and Mayford, M. (2007). Localization of a stable neural correlate of associative memory. Science *317*, 1230–1233.

Renier, N., Wu, Z., Simon, D.J., Yang, J., Ariel, P., and Tessier-Lavigne, M. (2014). iDISCO: a simple, rapid method to immunolabel large tissue samples for volume imaging. Cell *159*, 896–910.

Renwick, N., Cekan, P., Masry, P.A., McGeary, S.E., Miller, J.B., Hafner, M., Li, Z., Mihailovic, A., Morozov, P., Brown, M., et al. (2013). Multicolor microRNA FISH effectively differentiates tumor types. J. Clin. Invest. *123*, 2694–2702.

Resch-Genger, U., Grabolle, M., Cavaliere-Jaricot, S., Nitschke, R., and Nann, T. (2008). Quantum dots versus organic dyes as fluorescent labels. Nat. Methods *5*, 763–775.

Richardson, D.S., and Lichtman, J.W. (2015). Clarifying Tissue Clearing. Cell *162*, 246–257.

Shen, G., Anand, M.F.G., and Levicky, R. (2004). X-ray photoelectron spectroscopy and infrared spectroscopy study of maleimide-activated supports for immobilization of oligodeoxyribonucleotides. Nucleic Acids Res. *32*, 5973–5980.

Sheng, M., McFadden, G., and Greenberg, M.E. (1990). Membrane depolarization and calcium induce c-fos transcription via phosphorylation of transcription factor CREB. Neuron *4*, 571–582.

Simard, C., Lemieux, R., and Côté, S. (2001). Urea substitutes toxic formamide as destabilizing agent in nucleic acid hybridizations with RNA probes. Electrophoresis *22*, 2679–2683.

Smeyne, R.J., Schilling, K., Robertson, L., Luk, D., Oberdick, J., Curran, T., and Morgan, J.I. (1992). fos-lacZ transgenic mice: mapping sites of gene induction in the central nervous system. Neuron *8*, 13–23.

Spalteholz, W. (1911). Uber das Durchsichtigmachen von menschlichen und tierischen Präparaten und seine theoretischen Bedingungen (Leipzig: S. Hirzel).

Srinivasan, M., Sedmak, D., and Jewell, S. (2002). Effect of fixatives and tissue processing on the content and integrity of nucleic acids. Am. J. Pathol. *161*, 1961–1971.

Staudt, T., Lang, M.C., Medda, R., Engelhardt, J., and Hell, S.W. (2007). 2,2′-thiodiethanol: a new water soluble mounting medium for high resolution optical microscopy. Microsc. Res. Tech. *70*, 1–9.

Susaki, E.A., Tainaka, K., Perrin, D., Kishino, F., Tawara, T., Watanabe, T.M., Yokoyama, C., Onoe, H., Eguchi, M., Yamaguchi, S., et al. (2014). Whole-brain imaging with single-cell resolution using chemical cocktails and computational analysis. Cell *157*, 726–739.

Tainaka, K., Kubota, S.I., Suyama, T.Q., Susaki, E.A., Perrin, D., Ukai-Tadenuma, M., Ukai, H., and Ueda, H.R. (2014). Whole-body imaging with single-cell resolution by tissue decolorization. Cell *159*, 911–924.

Tomer, R., Ye, L., Hsueh, B., and Deisseroth, K. (2014). Advanced CLARITY for rapid and high-resolution imaging of intact tissues. Nat. Protoc. *9*, 1682–1697.

Tomer, R., Lovett-Barron, M., Kauvar, I., Andalman, A., Burns, V.M., Sankaran, S., Grosenick, L., Broxton, M., Yang, S., and Deisseroth, K. (2015). SPED light sheet microscopy: fast mapping of biological system structure and function. Cell *163*, 1796–1806.

Tymianski, M., Bernstein, G.M., Abdel-Hamid, K.M., Sattler, R., Velumian, A., Carlen, P.L., Razavi, H., and Jones, O.T. (1997). A novel use for a carbodiimide compound for the fixation of fluorescent and non-fluorescent calcium indicators in situ following physiological experiments. Cell Calcium *21*, 175–183.

Wanner, A.A., Kirschmann, M.A., and Genoud, C. (2015). Challenges of microtome-based serial block-face scanning electron microscopy in neuroscience. J. Microsc. *259*, 137–142.

Wernersson, R., Juncker, A.S., and Nielsen, H.B. (2007). Probe selection for DNA microarrays using OligoWiz. Nat. Protoc. *2*, 2677–2691.

Wilkinson, D.G. (1999). In Situ Hybridization: A Practical Approach (Oxford University Press).

Yang, B., Treweek, J.B., Kulkarni, R.P., Deverman, B.E., Chen, C.-K., Lubeck, E., Shah, S., Cai, L., and Gradinaru, V. (2014). Single-cell phenotyping within transparent intact tissue through whole-body clearing. Cell *158*, 945–958.

Zeisel, A., Muñoz-Manchado, A.B., Codeluppi, S., Lönnerberg, P., La Manno, G., Juréus, A., Marques, S., Munguba, H., He, L., Betsholtz, C., et al. (2015). Brain structure. Cell types in the mouse cortex and hippocampus revealed by single-cell RNA-seq. Science *347*, 1138–1142.

Zhou, R., Yuan, P., Wang, Y., Hunsberger, J.G., Elkahloun, A., Wei, Y., Damschroder-Williams, P., Du, J., Chen, G., and Manji, H.K. (2009). Evidence for selective microRNAs and their effectors as common long-term targets for the actions of mood stabilizers. Neuropsychopharmacology *34*, 1395–1405.

Supplemental Figures

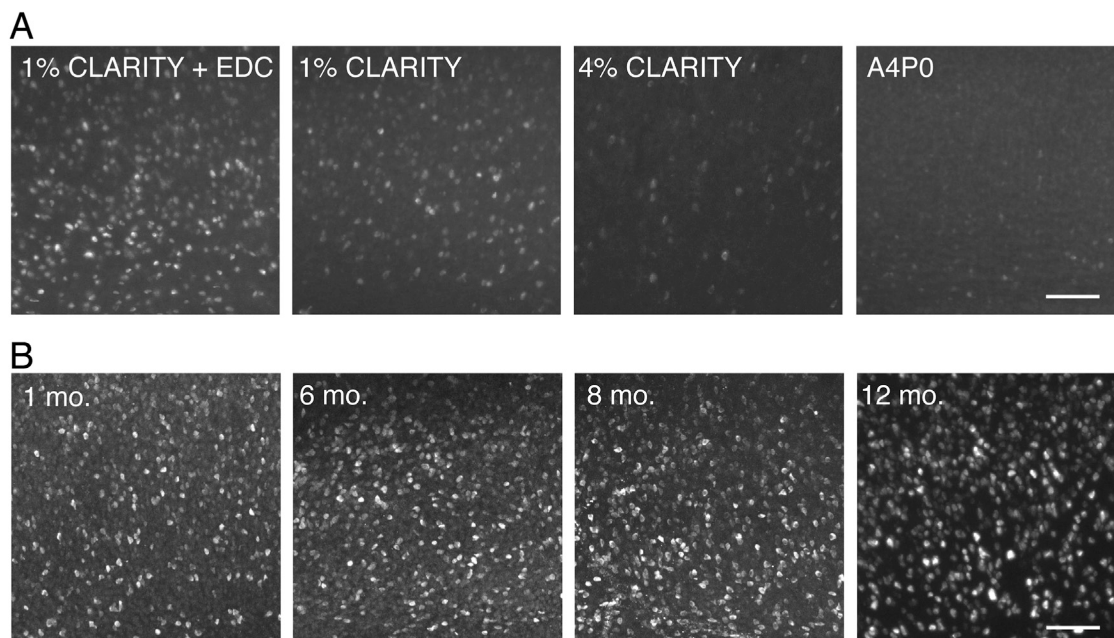

Figure S1. Characterization of Tissue Formulation and Storage Time for In Situ Hybridization, Related to Figure 1

(A) CLARITY sections (1 mm) of mouse tissue from cortex embedded in 1% CLARITY hydrogel, 4% CLARITY hydrogel, 1% CLARITY hydrogel with EDC postfixation, or A4P0 (4% acrylamide, no bis-acrylamide, no PFA during acrylamide polymerization), were cleared in 4% SDS until transparent, and in situ hybridization for *somatostatin* was performed on the cleared tissue. Images are maximum z-projections from 5 planes, z-interval = 20 μm. Scale bar, 100 μm.
(B) EDC-CLARITY sections (1 mm, 1% hydrogel) were cleared until transparent and stored in PBST for the times indicated. In situ hybridization for *somatostatin* was performed and confocal images were acquired. Images are maximum z-projections from 5 planes, z-interval = 20 μm. Scale bar, 100 μm.

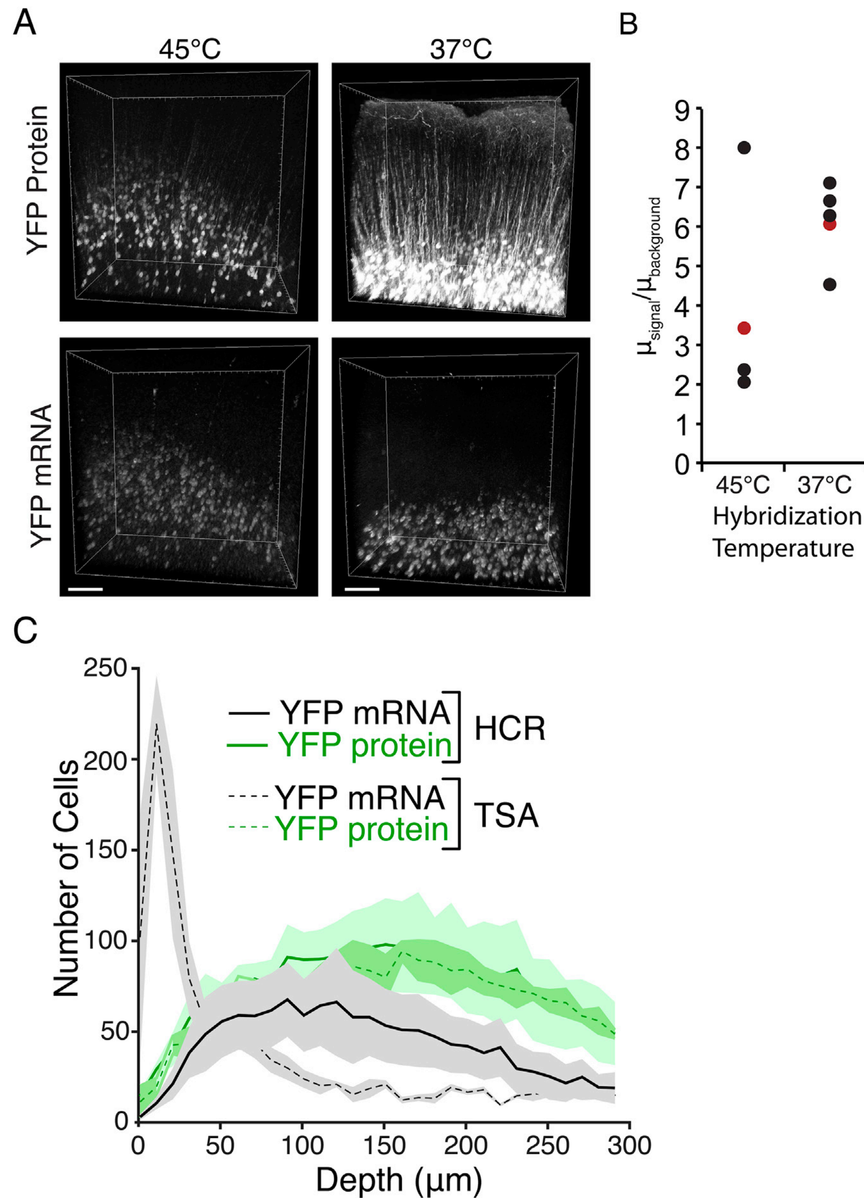

Figure S2. Validation of Amplification Specificity, Related to Figure 3

(A) EDC-CLARITY sections (1 mm) of tissue from Thy1-YFP mouse cortex. *YFP* probes were either hybridized at 45°C (50% formamide, 5x SSC) or at 37°C (40% formamide, 2x SSC) overnight and amplified using HCR. (Top) Three dimensional rendering of YFP fluorescence after in situ hybridization. (Bottom) Three dimensional rendering of *YFP* mRNA by HCR-based in situ hybridization. Scale bar, 200 μm.

(B) YFP fluorescence from EDC-CLARITY tissue after in situ hybridization at 37°C or 45°C, calculated as the ratio of mean intensity of signal to the mean intensity of the background. Each data point represents one volume. Representative volumes in (A) are indicated in red.

(C) EDC-CLARITY sections are hybridized with *YFP* probes labeled with either DIG or initiator sequences and amplified with TSA or HCR, respectively. Cells identified by YFP protein fluorescence (green) or *YFP* ISH (black) after local thresholding and cell segmentation are plotted against tissue depth; 10 μm z-interval. High background on tissue surface with TSA amplification produces many false positives 0-50 μm from the tissue surface that are not seen in the YFP protein controls (n = 3 for each condition, error bars represent SEM).

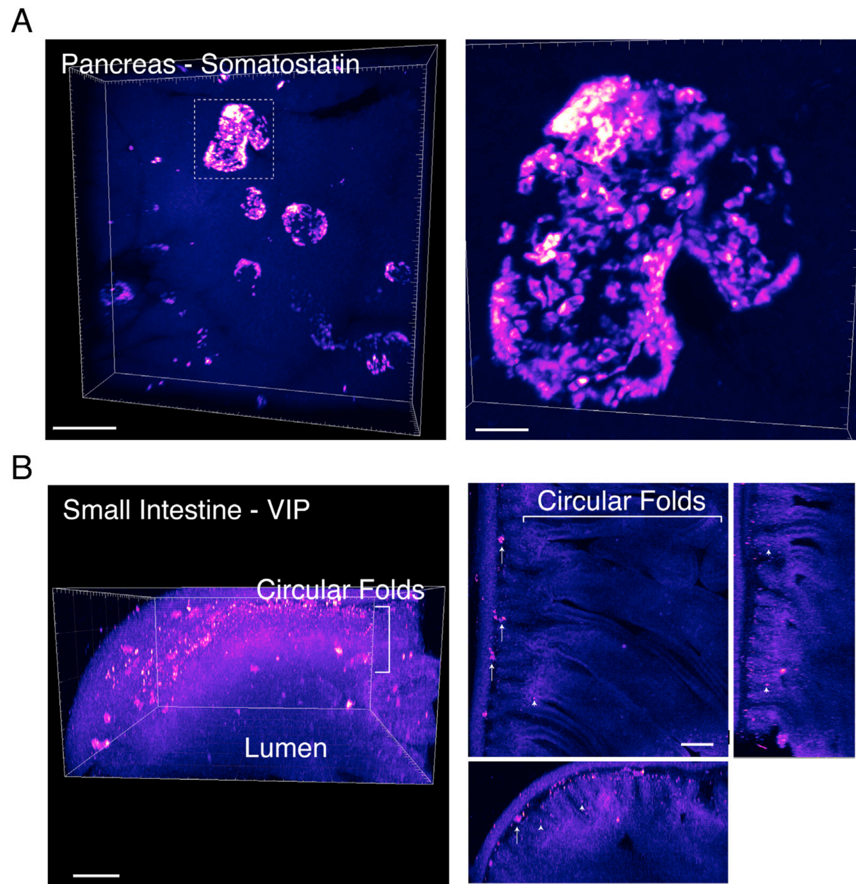

Figure S3. Application of EDC-CLARITY to Non-neural Tissue, Related to Figure 4

(A) Left, Three-dimensional rendering of a 1 mm thick EDC-CLARITY section of mouse pancreas with in situ hybridization for *somatostatin*. Scale bar, 300 μm. Right, expanded view of box at right. Delta cells in pancreatic islets are prominently labeled. Scale bar, 50 μm.

(B) Left, Three dimensional rendering of an EDC-CLARITY section of mouse small intestine with in situ hybridization for *VIP*. Scale bar, 100 μm. Right, orthogonal views of tissue at left. Large cells positive for *VIP* (arrows) are putative peripheral neurons in the submucosal plexus. Smaller puncta in the circular folds correspond well with the distribution of *VIP* expressing enteroendocrine cells (arrowheads). Scale bar, 200 μm.

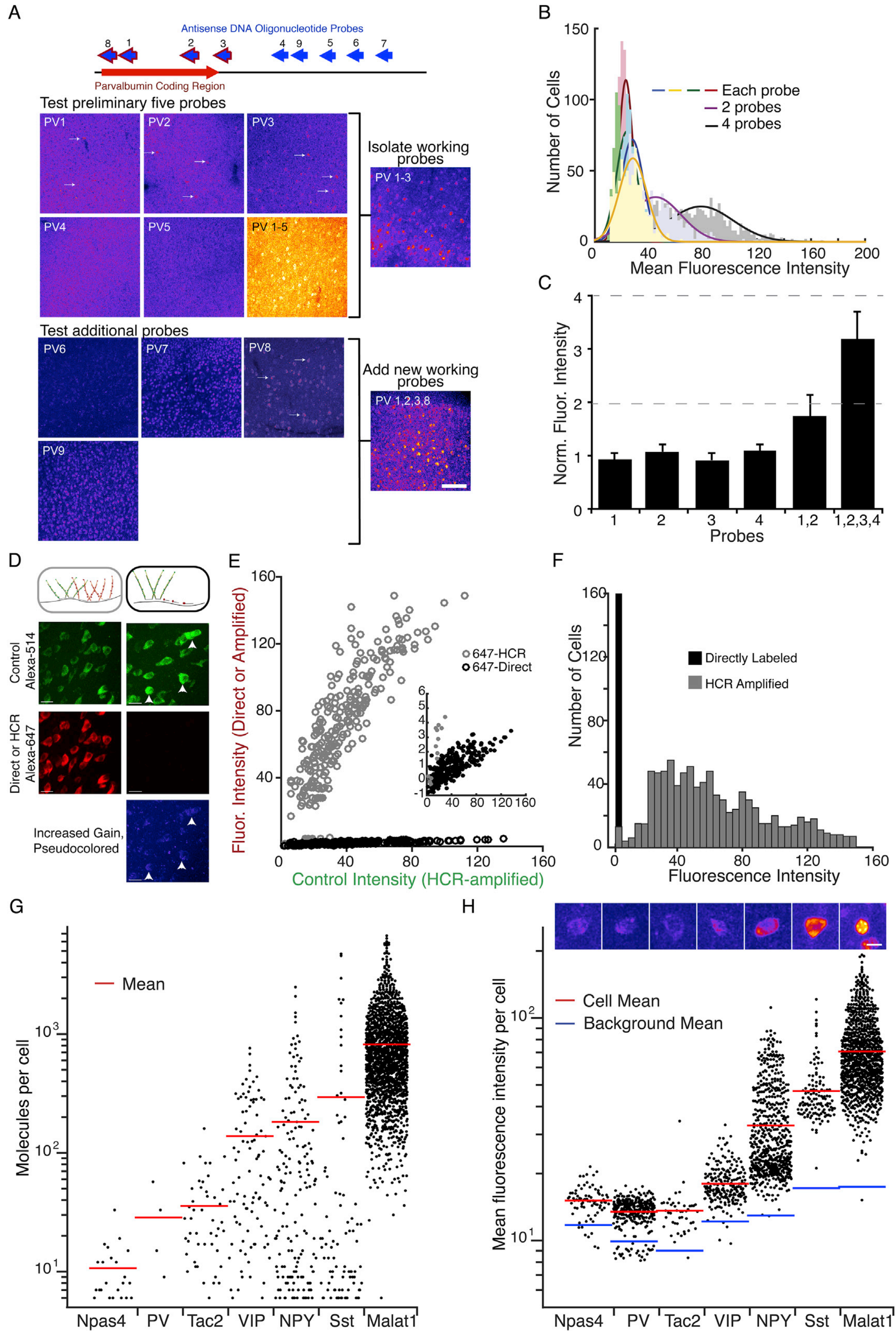

(legend on next page)

Figure S4. Characterization of HCR Probe Design and Amplification Sensitivity, Related to Figure 4

(A) In situ hybridization for *parvalbumin* in 500 μm EDC-CLARITY sections. Confocal images of *parvalbumin* ISH in cortex. Initial testing of 5 probe cocktail targeting *parvalbumin* (PV1-5) had high background. Probes were tested individually and probes 1-3 showed specific signal. Omitting probes 4 and 5 decreased background. A second set of 4 probes contains one specific probe (PV8). For *parvalbumin*, all working probes targeted the coding region of the mRNA. Blue arrows indicated probes tested, red outlines indicate successful probes. All scale bars, 100 μm.

(B) Histogram of cell fluorescence intensities for individual *somatostatin* probes, or combinations of 2 or 4 probes. In situ hybridizations were performed on 500 μm thick CLARITY-EDC sections and amplified with HCR. Cells are segmented, mean fluorescence intensity is plotted, and normal distributions are fit to the data. (n = 3 experiments).

(C) Average of mean cell intensities per experiment, from data shown in (B), normalized to the average of all individual probes (columns 1-4). Dotted lines represent the linear sum of 2 or 4 probes. (n = 3 experiments). Data are means ± SD.

(D) Estimation of fold amplification with HCR. 500 μm EDC-CLARITY tissue was hybridized under two conditions. In the first condition, one set of *somatostatin* probes is labeled with B1 initiators and another set targeting different sequences is labeled with B5 initiators. Both are amplified with HCR, but with different fluorophores: B1-Alexa647 and B5-Alexa514. In a second condition, one group of probes is labeled with B5 initiators amplified with Alexa514, but the other probes are labeled directly with Alexa647.

(E) S*omatostatin* containing cells were identified using the control Alexa514 channel and the mean fluorescence intensity for both channels was calculated for each cell (average background of each ROI was subtracted from mean intensity). Data for one representative experiment is plotted in (E) as the signal intensity in the Alexa647 channel (for either directly-labeled or HCR-amplified probes) as a function of the control HCR-amplified, Alexa514. Inset highlights low range of y axis.

(F) Histogram of fluorescence intensities of the Alexa 647 channel for directly labeled or HCR-amplified probes from 4 experiments as in (E). The ratio of the mean HCR value to the mean directly labeled value suggests that there is ∼50 fold amplification.

(G) Genes with mRNA copy numbers ranging over several orders of magnitude were selected from a published dataset in which single cell RNA-seq data were collected from 1,691 cells in mouse cortex (Zeisel et al., 2015). To compare with our dataset, which predominantly uses interneuron cell markers that are highly expressed in one subpopulation but much lower elsewhere, we excluded cells in the RNA-seq dataset corresponding to detection of fewer than 5 molecules. Red bars indicate the mean of all cells with > 5 transcripts of the gene indicated.

(H) In situ hybridizations for 7 different mRNAs were performed in parallel on 500 μm EDC-CLARITY sections of cortex with comparable ROIs taken with identical imaging parameters. To improve cell identification for more weakly expressing mRNAs, images were first acquired at the same gain, and then weak signals were imaged again at increased gain. High gain was used to detect cells, but all measurements are from the low gain images, which were the same across all transcripts. Representative cells are shown in the inset and pseudocolored. Below, mean fluorescence intensities are plotted for all cells from three separate experiments, using the same imaging and cell detection parameters for each mRNA. For ease of visualization, a random subset of 1,000 cells is shown for *Malat1*. Red bars indicated the mean intensity for segmented cells; blue bars indicate mean background fluorescence. We are able to detect *Npas4* expressing cells, which RNA-seq data from Zeisel et al. (2015) suggests contain ∼50 copies of *Npas4* per cell (average molecules detected is ∼10, adjusted for a 22% capture rate).

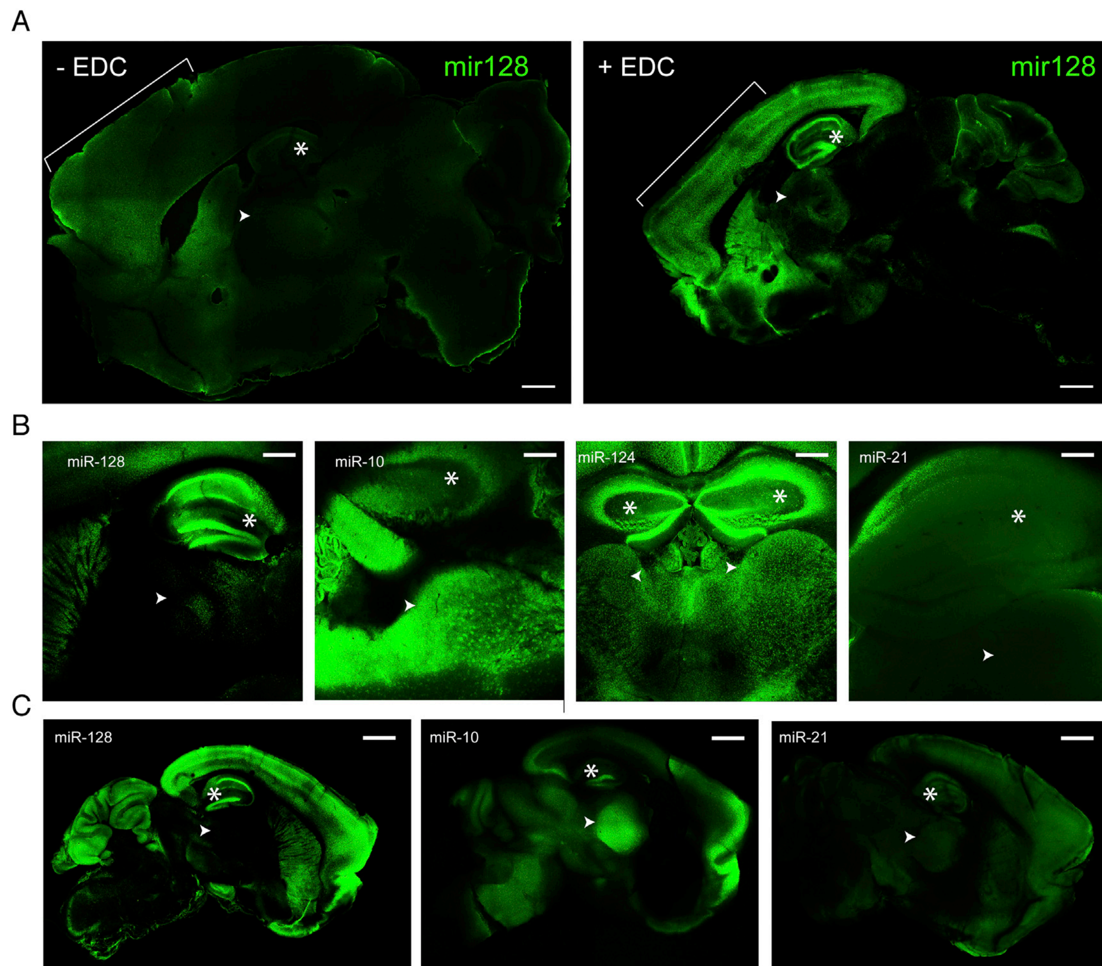

Figure S5. Detection of microRNAs in CLARITY Tissue, Related to Figure 5

(A) Projection images of 5x confocally acquired and tiled 1 mm mouse brain sagittal sections, cleared, and in situ hybridized with DIG-labeled LNA probes complementary to the mature *miR-128* sequence without (left) and with (right) EDC fixation. Brain regions indicated as follows: forebrain (brackets), hippocampus (asterisk), thalamus (arrowhead). Scale: 700 μm (left) and 800 μm (right).

(B) Projection images of 10 × confocally acquired 1 mm mouse brain coronal sections, cleared and in situ hybridized with DIG-labeled LNA probes complementary to the mature *miR-128*, *miR-10b*, *miR-124*, and *miR-21* sequences. *miR-128* is preferentially expressed in hippocampus (asterisk), miR-10 in thalamus (arrowhead), and *miR-124* in both. There is minimal expression of *miR-21* in either structure (consistent with sequencing data suggesting lack of *miR-21* expression in adult brain tissue). Scale: 100/100/100/50 μm.

(C) Projection images of 5 × confocally acquired and tiled 1 mm mouse brain sagittal section, cleared and in situ hybridized with DIG-labeled LNA probes complementary to the mature *miR-128*, *miR-10*, and *miR-21* sequences. Scale: 150 μm. Brain regions indicated as follows: hippocampus (asterisk), thalamus (arrowhead).

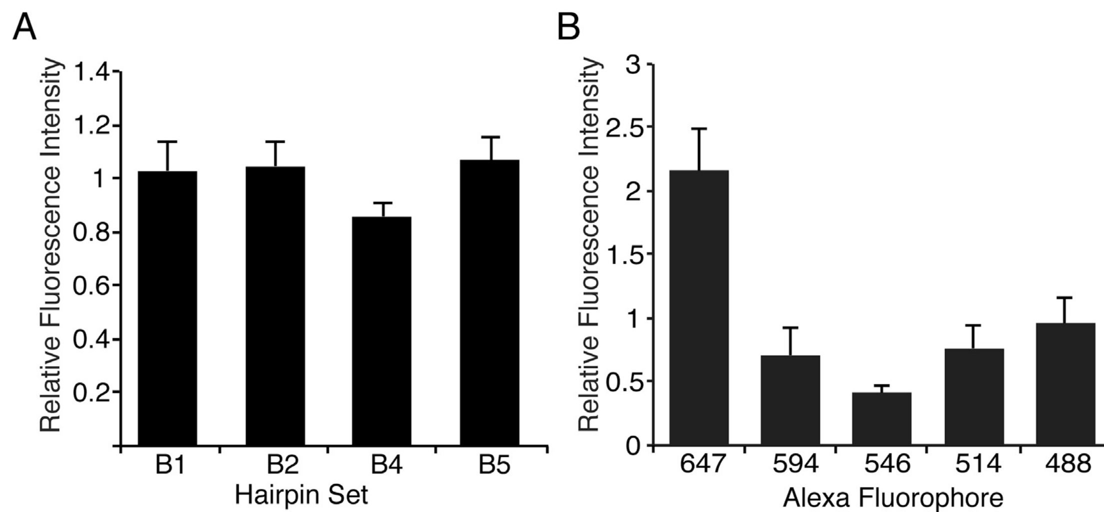

Figure S6. Characterization of Orthogonal Hairpins, Related to Figure 6

(A) Four orthogonal hairpins sets have equivalent amplification in CLARITY-EDC tissue. In situ hybridizations for *somatostatin* were performed using the same probe sequences and fluorophore (Alexa647), with 4 different hairpin sets (B1, B2, B4, and B5, as described in Choi et al. (2014), and normalized to the mean intensity of all conditions (n = 3) Data are means ± S.D.

(B) Relative fluorescent intensities of different Alexa fluorophores. In situ hybridization for *somatostatin* was performed on 500 μm CLARITY tissue using B1 hairpins conjugated to the dyes indicated. Fluorescence intensity of *somatostatin* cells was calculated, background auto fluorescence was subtracted for each channel, and then normalized to the mean intensity of all conditions (n = 3) Data are means ± SD.

Cell, Volume *164*

Supplemental Information

Multiplexed Intact-Tissue Transcriptional

Analysis at Cellular Resolution

Emily Lauren Sylwestrak, Priyamvada Rajasethupathy, Matthew Arnot Wright, Anna Jaffe, and Karl Deisseroth

SUPPLEMENTAL EXPERIMENTAL PROCEDULES

CLARITY Tissue Preparation. CLARITY tissue was prepared as described in (Tomer et al., 2014). In brief, C57/Bl6 8-12 weeks of age were anaesthetized with beuthanasia (100 mg/kg) and transcardially perfused with cold PBS, followed by cold hydrogel solution (1% or 4% acrylamide, 0.0125% bisacrylamide (for 1% acrylamide) or 0.05% bisacrylamide (for 4% acrylamide), 0.25% VA-044 initiator, 1x PBS, 4% PFA in dH_2O). Tissues were removed and post-fixed overnight at 4^oC. For induction of immediate early genes, animals were injected with either saline or kainic acid (12mg/kg, i.p.) 2 hours prior to perfusion and monitored for seizure activity. For A4P0 samples, tissues were first perfused in 4% PFA, post-fixed in 4% PFA for 24h (4°C), then transferred to a PFA-free embedding solution (4% acrylamide, 0.25% VA-044 initiator, 1x PBS in dH_2O) for 48h. Conical tubes containing samples were degassed under vacuum for 10 minutes, chamber was flooded with nitrogen, oil was quickly added to the surface of the hydrogel solution and tubes were immediately capped. Gel was polymerized at 37°C for 5 hours, removed from hydrogel solution and sectioned where indicated using a vibratome (500 µm sections) or sectioning block (1, 2, or 3mm sections). Additional fixatives (EDC, PMPI, or DSS) were added, as indicated. Tissue was cleared passively in a 4%SDS/ 0.2M Boric acid (pH=8.5) clearing solution at 37 ^oC with gentle shaking (0.5mm, ~1 week; 1mm, 1-2 weeks; 2-3mm, ~3 weeks). Clearing solution was changed every 1-2 days. Cleared tissue was washed three times (1 hour each), plus overnight, and stored in 1x PBS with 0.3% TX-100.

RNA fixation. Fixation with EDC, PMPI, and DSS was performed after hydrogel embedding, prior to clearing. For EDC fixation, tissue sections were incubated for 30 minutes in methylimidazole buffer (0.1M, pH 8.5) and transferred to 500 µl EDC fixative solution (0.1M 1-ethyl-3-(3-dimethylaminopropyl) carbodiimide, 0.1M 5-Ethylthio-1H-tetrazole, in 0.1M methylimidazole buffer, pH to 8.5). For PMPI fixation, tissue sections were incubated in 500 µl of 0.1M N-[p-maleimidophenyl] isocyanate in DMSO, pH to 8.5; and for DSS fixation, tissue sections were incubated in 500 µl of 0.1M of disuccinimidyl suberate in DMSO, pH to 8.5. For all fixatives, sections were light protected and incubated overnight at 37^oC, then transferred to clearing solution. For further characterization of the EDC fixative, sections were incubated in varying concentrations of the fixative (0, 0.1M, 1M, 10M) for varying durations (3h or overnight) at 37^oC, then transferred to clearing solution.

Total RNA isolation and acridine orange staining. Cleared tissue was homogenized in 20 µg/ml proteinase K (100 µl total volume per 1mm tissue) and incubated on a 50°C shaker for 3h. RNA was extracted according to the standard Trizol (Invitrogen) protocol, followed by an additional acidic phenol:chloroform:isoamyl alcohol extraction (equal volume of Ph:Chl:IAA) for separation of RNA from DNA, followed by a final chloroform extraction (equal volume of Chl). The resulting aqueous layer was transferred to a new 1.5mL falcon tube, with addition of 1/10 volume of 3M sodium acetate as a carrier for precipitation, reaching a final concentration of 0.3M salt. The RNAs were then precipitated in 3 volumes of ethanol, for at least one hour at -20°C, and then recovered as a pellet by centrifuging at 12,000 RPM at 4°C. The supernatant was removed, pellet was washed in 70% ethanol, allowed to air dry, re-dissolved in 10 µl of ultrapure water, and quantified by nanodrop.

For staining of total RNA by acridine orange, tissue sections were rinsed in SC buffer (0.1M citric acid, 0.2M sodium phosphate dibasic, pH 4.0) for 10 minutes, then incubated in 1 mL of acridine orange solution (100 ug AO in 1 mL SC buffer) for three hours, then rinsed three times for 30 minutes each in SC buffer, before finally rinsing in PBS, and refractive index matching in FocusClear.

Probe Design. For riboprobes, (Figure 2B,C), cDNA templates for *somatostatin* (Probe #1, Genbank: BC010770, 280-429) or *parvalbumin* (Probe #2, Genbank: BC027424, 203-352) were generated by Genscript. Vectors were linearized and reverse transcribed using T7 RNA polymerase and DIG-labeled dNTPs (Roche), and purified by phenol chloroform extraction. smFISH probes (Figure 4J-L) were designed and synthesized by Biosearch Technologies (Petaluma, CA). DNA 50mer initiator-labeled oligonucleotide probes (Figure 3-5) were either purchased from Molecular Instruments (Pasadena, CA; *Parvalbumin*, *Tac1*, *Th*, 10 probes each), or designed using OligoWiz software (Wernersson et al., 2007) and synthesized by Integrated DNA Technologies (Figure 4 and 5, *somatostatin*, *NPY*, *VIP*, *Tac2*, *Malat1*, *Npas4*, *Arc*, 4-6 probes each). LNA probes were synthesized by Exiqon (Figure 5).

Probe and Antibody Diffusion. For experiments comparing RNA and DNA probe diffusion (Figure 2B,C), coronal sections of cleared tissue (2mm) were incubated in 50% formamide, 5x SSC for 3 hours at 55°C in 0.5ml eppendorf tubes. These conditions were used because they produced successful *in situ* hybridization with both DNA and RNA probes in parallel experiments. Tubes were cooled to 4°C for 15 min to allow for non-specific binding of probe in

order to better immobilize probe for PFA fixation. Sections were postfixed overnight in 4% PFA, washed in PBST, embedded in 2% agarose, and re-sectioned (200µm) on a vibratome. Cross-sections of the center of tissue were selected for staining and transferred to PBST containing anti-DIG antibody conjugated to HRP (1:1000) for 1 hour at room temperature. Sectioning tissue in this way allowed us to eliminate the contribution of inhomogeneities in antibody or TSA diffusing by performing these steps directly on the newly exposed tissue surface. Antibody was washed (3x15 minutes) and tissue was transferred to TSA (1:200) for 5 minutes, washed in PBST, and mounted in PBS. The surface of each cross section was imaged by confocal microscopy, and 2-3 RIOs containing the tissue edge from each section were quantified, taking care to select regions of homogeneous tissue lacking major fiber tracts.

For experiments comparing DNA oligonucleotide diffusion at different time points (Figure 2E), tissue was incubated in 40% formamide and 2x SSC at 37°C for 30, 60 or 180 minutes. Temperature and formamide concentration were reduced to reflect the conditions optimized for DNA hybridization and preservation of endogenous YFP fluorescence used in subsequent experiments.

For experiments measuring antibody diffusion, tissue was incubated in 50mer DIG-labeled oligonucleotides overnight in 40% formamide and 2xSSC (probe distribution is mostly uniform at this point). The tissue was cooled to 4C for 15 minutes to immobilize probe and crosslinked in 4% PFA for one hour at room temperature. The tissue was then incubated with anti-DIG Fab fragment antibody coupled to HRP (1:1000) in PBST for the corresponding time and tissue was further processed as above for re-sectioning and TSA amplification.

***In situ* hybridization**. For Oligo(dT) *in situ* hybridization (Figure 1), cleared tissue was equilibrated in hybridization solution (15% deionized formamide, 2x SSC, 10% dextran sulfate) for 1 hour. Tissue was hybridized in the same solution containing oligo(dT) probe (50nM, 50 base deoxy thymine probe conjugated to Cy5) overnight at 37°C. Stringency washes: 3 x 1 hour (15% formamide, 2x SSC) and 2 x1 hour (2x SSC). For Propidium Iodide stain, tissue was incubated in PropI/RNase solution for 1 hour and then washed with 2xSSC 3x1 hour. Sections were transferred to FocusClear for 4 hours prior to imaging.

For *in situ* hybridization with DIG-labeled 50mer DNA oligonucleotides (Figure 3), cleared tissue was equilibrated in hybridization solution (50% deionized formamide, 5x SSC, 0.5mg/ml yeast tRNA, 10% dextran sulfate) for 1 hour. Tissue was hybridized in the same buffer containing 50nM DIG-labeled DNA probe to target in addition to 10nM N50 oligo to reduce nonspecific binding overnight at 55 °C. Stringency washes: 3 x 1 hour (50% formamide, 5x SSC), 2 x 1 hour in 2x SSC. Tissue was transferred to PBST (0.3% TX-100 in 1x PBS) and washed twice, 1 hour each. Sections were incubated with anti-DIG antibody conjugated to HRP (Roche, 1:500 dilution) for 2d per mm tissue thickness, washed overnight in PBST. TSA amplification reaction was performed at 1:50 dilution in commercial buffer for 30 minutes, washed in PBST and transferred to FocusClear for imaging.

For microRNA *in situ* hybridization with DIG-labeled LNA probes, cleared tissue was rinsed in PBST (0.3% TX-100 in 1x PBS) for at least one night, then incubated in hybridization solution overnight (1 mL of hybridization solution consisting of 50% deionized formamide, 5x SSC, 0.5 mg/ml yeast tRNA, and 12.5 nM probe labeled on both ends with DIG). Probe hybridization was performed at a temperature that is 20 degrees below the Tm of the probe (usually between 45 to 55 °C, avoiding incubation temperatures above 55 °C). We noticed good signal to noise even at temperatures as low as 37 °C). Stringency washes: 2x 1 hour (5x SSC), then 1x 1 hour (1x SSC). Signal amplification with TSA and refractive index matching with FocusClear were performed as described above.

For *in situ* hybridization with initiator-tagged 50mer DNA oligonucleotides (Figure 3-6), cleared tissue was equilibrated in hybridization solution for one hour (40% deionized formamide, 2x SSC, 0.5mg/ml yeast tRNA, 10% dextran sulfate). Tissue was hybridized in the same buffer containing 0.5-4nM initiator-labeled probe overnight at 37°C (See Supplemental Table 1 for probe concentrations). Stringency washes: 3x 1 hour (40% formamide, 2x SSC) with an additional overnight wash for sections thicker than 1 mm). Tissue was then transferred to 5x SSCT (5x SSC, 0.1% Tween 20) and washed twice, 1 hour each. Sections were pre-incubated in amplification solution for 30 min (5x SSC, 10% dextran sulfate, 0.1% Tween 20). 3 µM stock hairpin solutions were separately diluted in 20x SSC (for a final concentration of 2.25 µM hairpin in 5x SSC) and heated to 90°C for 90 seconds, then cooled bench top for 30 min. Cooled hairpins were transferred to amplification buffer (120-240 nM final concentration) and tissue was incubated in amplification buffer with hairpins for 1-2 days at room temperature. Tissue was washed in 5x SSCT 5x1 hour (overnight for sections over 1 mm) and transferred to FocusClear for 4 hours prior to imaging.

An exception to the protocol above is the HCR experiment in Figure 3D, in which some hybridizations were performed in 50% formamide, 5xSSC, 0.5mg/ml yeast tRNA, 10% dextran sulfate, at 55C and stringencies in 50% formamide and 5xSSC to directly compare with their TSA counterparts. There was no significant difference between HCR hybridizations for *somatostatin* performed under the two conditions (other probe sets were not tested at the 50% formamide condition).

For *in situ* hybridization with smFISH probes bearing the initiator sequences on the 5' end, procedure was the same as above, but with a hybridization solution containing 10% formamide, 2x SSC,10% dextran sulfate and 5nM N20 oligo; stringency washes were with 10% formamide in 2x SSC.

Human Tissue. Human tissue was obtained from 2 surgical patients. Both samples are putative healthy tissue from surgical corridors of temporal lobe resections for epilepsy treatment. For the first patient (46 y.o. female), tissue was collected and transferred to PFA <2 hours after removal, fixed overnight in PFA, transferred to 1% hydrogel solution for 2 days at 4°C, polymerized for 5 hours at 37 °C, and cleared for 5 weeks in 4% SDS. The second sample (18 y.o. male) was removed and placed in oxygenated solution for 2 hours in the presence of AP5, CNQX, Gabazine, then transferred to 1% hydrogel solution for 2 days at 4°C, polymerized for 5 hours at 37 °C, fixed overnight in EDC at 37°C, and cleared for 5 weeks in 4% SDS at 37°C.

Confocal Microscopy. All images were taken on a Leica SP5 confocal microscope with a 10x/0.4 objective (WD: 2.2 mm) or 20x/0.75 objective (WD: 0.66 mm) at 488 nm (FITC), 514 nm, 543 nm, or 633 nm excitation. Tissue shrinks once equilibrated to FocusClear for imaging, and all scale bars represent the imaged volume, which is approximately 50% of original tissue volume. Tissue sections were sandwiched between a glass slide and coverslip, using sticky tack as a spacer, and the chamber was filled with refractive index matching solution (FocusClear), as previously described in (Chung et al., 2013).

Image Analysis. For comparisons between HCR and TSA amplification (Figure 3), images were acquired at 10 µm intervals and analyzed using Fiji software. Individual xy planes were locally thresholded using a mid-gray filter and the resulting particles were filtered by size and circularity in order to eliminate axons and dendrites in Thy1-YFP cell detection. We selected the z=0 imaging plane to be the first imaging plane containing tissue, but CLARITY tissue surfaces are not completely uniform, resulting in initial z planes that contained tissue in only part of the field of view, which account for the gradual rise in signal over the first 50µm of tissue depth. Signal to background ratios were determined by calculating the ratio of mean fluorescence intensity of all cells detected in each xy plane to the mean intensity of the rest of the image. For Sst-TFP (Figure 3F), this may underestimate the signal to background ratio, since TFP is cytosolic and some dendrites will be included in the background measurement.

For three-dimensional volumetric rendering (Figures 4-6), confocal images were acquired at 5 µm or 10 µm intervals and analyzed using Imaris software (BitPlane). For tiled images, tiles were assembled by Leica acquisition software (SP5) before exporting to Imaris. To analyze the number of cells detected in these volumes (Figure S4), we used Imaris cell detection algorithms (spots) to identify and quantify cell number. For comparisons of HCR to directly labeled fluorophores (Figure S4E), cell detection was performed in the control HCR channel (Alexa514), and then fluorescence intensity of both channels was measured in the resulting cell boundaries. Using 50 hand-annotated ROIs containing only background, mean background fluorescence was calculated and subtracted from the data set for each channel. For comparisons to RNA-seq data (Figure S4H), all samples from a given experiment were processed in parallel. A low gain condition was chosen which did not saturate in the highest expressing transcript, *Malat1*. All images were acquired first at low gain, and then low expressing transcripts were imaged again at a higher gain to facilitate cell identification. After identifying the cells, all subsequent calculations used the low gain images. For comparing fluorophores and hairpins (Figure S6), volumes were captured and cells segmented using Imaris software (spots). To compare fluorophores more directly, the mean intensity value from 50 hand-annotated ROIs corresponding to known background was subtracted from each condition to normalize for differences in tissue autofluorescence at each wavelength.

EDC-CLARITY PROTOCOL, related to Experimental Procedures
CLARITY Tissue Preparation for *In Situ* Hybridization
Passive tissue clearing is performed as described in Tomer et al. Nature, 2014. In brief:

1. Perfuse animal with cold PBS, then cold CLARITY hydrogel solution:

Hydrogel Solution

Chemical	Volume in 400ml	Final Concentration
Acrylamide (40%)	10 mL	1% final conc
Bis-acrylamide (2%)	2.5 mL	0.00125 % final conc
VA-044 Initiator	1 g	0.25% final conc
10X PBS	40 mL	1X
16% PFA	100 mL	4%
d H_2O	247.5 mL	-

2. Postfix brain in 20ml of hydrogel solution at 4°C overnight.

3. Degas solution under vacuum to remove dissolved oxygen, which inhibits polymerization. This can be done by degassing, flooding the chamber with nitrogen, then quickly capping the tube. *We have found that degassing under vacuum and then covering the hydrogel solution with a thin layer of sunflower oil (to slow any oxygen in the headspace from dissolving into the solution) has been helpful.*

4. Incubate 5 hours at 37°C

5. Section tissue, if applicable.

6. Transfer tissue to methylimidizole buffer (80µl methylimidizole in 10ml water) for 15 minutes.

7. Incubate tissue in EDC solution at 37°C o/n. This compound acts as a fixative for 5' terminal phosphates (Pena et al., 2009; Tymianski et al., 1997) . This fixative is particularly helpful in preserving and detecting small RNAs, but also increases retention of mRNAs. To note: EDC fixation will increase clearing time by few days.

EDC Fixative Solution

Chemical	Mass in 10ml	Final Concentration
EDC	0.19g	0.1M
ETT	0.13g	0.1M
Methylimidizole Buffer (80µl Methylimidizole in 10 ml in H_2O	80 µl	

pH to 8.5 with NaOH. pH is critical; EDC will precipitate if pH is too low, or if phosphate buffer is inadequately washed out.

8. Move post-fixed sections to clearing solution. Passive clearing in 4%SDS/ 0.2M Boric acid (pH=8.5) clearing solution at 37°C until clear. Switch out solutions everyday for at least first few days, then every other day should suffice.

Clearing Solution

Chemical	Mass in 1L	Final Concentration
Sodium tetraborate	40.24	0.2M
SDS	40g	4%
H_2O	1L	-

pH to 8.5 with NaOH.

9. After clearing, wash 3x in PBST (PBS + 0.3% Triton), 1 hour each, at RT and once overnight.

***In situ* hybridization in CLARITY – TSA Amplification**

The following protocol is for DIG-labeled riboprobes and end-labeled DNA or LNA oligonucleotides. If you already have these types of probes working for your targets of interest, this approach may be easiest to implement, as long as the volumes are small, since antibody penetration into EDC-CLARITY tissue is slower than nucleic acid diffusion.

1. Quench with 1%H_2O_2 in PBST at RT overnight.

2. Wash 3 x in PBST (30min - 1h ea) at RT.

3. Pre-incubate in hybridization solution 1 hour.

4. Hybridize probe in hybridization solution overnight.

   Hybridization should be done at temperatures 10-20deg below Tm of the selected probes; individual optimization might be necessary. We have had success with 50-mer DNA probes, 20-mer LNA probes, and hydrolyzed riboprobes spanning 100-1000bp. For 50mer DNA probes, we selected sequences that minimize secondary structure and cross hybridization, and have similar Tms by using OligoWiz (Wernersson et al., 2007). For LNA probes, we used Exiqon probe selection algorithms. Individual hybridization conditions are listed in Supplementary Table 1 and online at http://wiki.claritytechniques.org/index.php/ISH and www.clarityresourcecenter.org.

   Hybridization Solution

Chemical	Volume in 10ml	Final Concentration
Deionized Formamide	5ml	50%
20x SSC	2.5ml	5x
Yeast tRNA (10mg/ml)	0.5ml	0.5mg/ml
dH_2O	2ml	-

   *For 50mer DNA oligonucleotide probes, we included an N50 oligo to reduce non-specific hybridization.

5. LNA 20mer: Wash twice in 5xSSC (1h ea), and once in 1xSSC (1h) at hybridization temperature.

   DNA 50mer: Wash three times in 5xSSC plus 50% formamide (1h ea), and twice in 2xSSC (1h) at hybridization temperature.

6. Rinse in PBST at 37°C (30min).

7. Anti-DIG-POD Fab fragment antibody (Roche) in PBST 37°C (1:500) o/n.

8. Wash with PBST 3 x (60 min ea) RT, plus overnight.

9. TSA reaction (Perkin Elmer, TSA Plus Fluorescein).

   Dilute fluorescein 1:50 and incubate tissue section for 30 minutes.

10. Wash with PBST, 3 x 60 min ea. at RT.

11. Focus Clear (4h-o/n), ready for mounting/imaging.

***In situ* hybridization in CLARITY – HCR Amplification**

To be able to multiplex RNA targets more effectively, and make staining more uniform, we adapted the hybridization chain reaction (HCR) amplification for use in CLARITY tissue (Choi et al., 2010, Choi et al., 2014). This method allows for simultaneous and orthogonal detection of several RNA targets. Importantly, the components are DNA-based and are all under ~150bases, which allows for more even diffusion and a more uniform staining. Although this amplification technique has reduced background and improved tissue penetration, it relies heavily on a good set of DNA oligonucleotide probes. We either purchased probe sets directly from Molecular Instruments (Caltech) or we have used OligoWiz software to design our own. We use probes approximately 50 nucleotides long and started with sets of 3-5 probes, each containing initiator sequences on both 5' and 3' ends. Sequences were chosen to generate non-overlapping probes with low secondary structure and cross-hybridization, and that have similar Tms. If signal was weak, we increased the number of probes to 10 per target. If background is high in initial screening, we have found that testing individual probes to remove those contributing to non-specific staining is very

helpful. Probe concentration may need to be modified for each probe set. Once a good probe set is identified, we perform the EDC-CLARITY in the following way:

1. Incubate in probe hybridization buffer without probe for 1 hour.

2. Transfer to hybridization solution with probe. Hybridize overnight (37°C unless otherwise noted).

Hybridization– 50mer DNA oligonucleotides

Chemical	Volume in 10ml	Final Concentration
Deionized Formamide	4ml	40%
20x SSC	1ml	2x
Yeast tRNA (mg/ml)	0.5ml	0.5mg/ml
Dextran Sulfate (50%)	2ml	10%
dH_2O	2.5ml	-

Probe concentration varies with target and may need optimization. Concentrations used in this paper are indicated in Supplemental Table 1.

Hybridization– smFISH 20mer probe sets

Chemical	Volume in 10ml	Final Concentration
Deionized Formamide	1ml	10%
20x SSC	1ml	2x
Dextran Sulfate (50%)	2ml	10%
dH_2O	6ml	-

**Biosearch Technologies(Petaluma, CA) has designed the 20mer probe sets described in this study, which include 30-50 probes per mRNA target.*

Probe concentration varies with target and may need optimization. Concentrations used in this paper are indicated in Supplemental Table 1 and online at *at* http://wiki.claritytechniques.org/index.php/ISH and clarityresourcecenter.org.

3. Perform 3x1hour stringency washes at hybridization temperature with the solution listed below. If tissue section is > 1mm, an overnight stringency may be necessary.

50mer Oligonucleotide Stringency Solution

Chemical	Volume in 10ml	Final Concentration
Deionized Formamide	4ml	40%
20x SSC	1ml	2x
dH_2O	5ml	-

20mer smFISH Stringency Solution

Chemical	Volume in 10ml	Final Concentration
Deionized Formamide	1ml	10%
20x SSC	1ml	2x
dH_2O	8ml	-

Perform additional 2x 1 hour wash with 5xSSCT at room temperature.

5xSSCT

Chemical	Volume in 40ml	Final Concentration
20x SSC	10	5x
Tween20 (10%)	400µl	0.1%
dH2O	29.6ml	-

4. Pre-incubate in amplification buffer, 1 hour.

Amplification Buffer

Chemical	Volume in 40ml	Final Concentration

20x SSC	10	5x
Tween20 (10%)	400μl	0.1%
Dextran Sulfate (50%)	8ml	10%
dH2O	21.6ml	-

5. Snap Cool Hairpins:

   For 300μl of amplification buffer (120 nM):

   12μl of 3μM Hairpin 1 + 4 μl of 20xSSC in PCR tube
   12μlof 3μM Hairpin 2 + 4μl of 20xSSC in PCR tube
   Heat both tubes to 95°C for 90 seconds, cool to room temperature 30 minutes.
   Add both hairpins to 300μl amplification buffer in Eppendorf tube.
   For B1 hairpins with Alexa647, we use 120nM. For B2-Alexa543 and B5-Alexa514 hairpins we use 240nM.
   Transfer CLARITY tissue to hairpin solution, incubate overnight at room temperature. For tissue >2mm thick, it may helpful to incubate for 2 days.
6. Wash 5 x 1 hr with 5xSSCT at RT, plus one wash overnight if >1mm thickness.

Transfer to refractive index matching solution; wait until transparent (1-4 hours). Signal is stable in FocusClear 1-2 days. Signal is stable for longer periods in ScaleA2, RIMS, or Glycerol, but sample transparency suffers, so may be suitable for <1mm sections, but not for larger volumes. Larger volumes can be challenging to make transparent again during refractive index matching. During hybridization and stringency, the tissue shrinks considerably. For tissue >2mm thick, we've found it helpful to re-expand the tissue before refractive index matching. For the 3mm section in Supplemental Movie 4, we transferred the tissue from 5xSSCT (after hairpin amplification) back to clearing solution (4% SDS in 0.2M borate buffer, 37 ^{o}C) overnight, then wash three times with 0.2M borate buffer to remove SDS. The expanded tissue equilibrates to RI matching in FocusClear more quickly and more thoroughly.